AERO-ASTRONAUTICS REPORT NO. 250

DECOMPOSITION TECHNIQUE AND OPTIMAL TRAJECTORIES FOR THE AEROASSISTED FLIGHT EXPERIMENT

by

A. MIELE, T. WANG, AND A. W. DEATON

RICE UNIVERSITY

1990

AERO-ASTRONAUTICS REPORT NO. 250

DECOMPOSITION TECHNIQUE AND OPTIMAL TRAJECTORIES FOR THE AEROASSISTED FLIGHT EXPERIMENT

by

A. MIELE, T. WANG, and A. W. DEATON

RICE UNIVERSITY

1990

Decomposition Technique and Optimal Trajectories for the Aeroassisted Flight Experiment[1]

by

A. Miele[2], T. Wang[3], and A. W. Deaton[4]

[1]This research was supported by NASA Marshall Space Flight Center Grant No. NAG-8-820, by Jet Propulsion Laboratory Contract No. 956415, and by Texas Advanced Technology Program Grant No. TATP-003604020.

[2]Foyt Family Professor of Aerospace Sciences and Mathematical Sciences, Aero-Astronautics Group, Rice University, Houston, Texas.

[3]Senior Research Scientist, Aero-Astronautics Group, Rice University, Houston, Texas.

[4]Aerospace Engineer and Team Leader, Flight Mechanics Branch, Systems Analysis and Integration Laboratory, NASA Marshall Space Flight Center, Huntsville, Alabama.

Abstract. The aeroassisted flight experiment (AFE) refers to a spacecraft to be launched and then recovered by the space shuttle in 1994. It simulates a transfer from a geosynchronous Earth orbit (GEO) to a low Earth orbit (LEO). Specifically, the AFE spacecraft is released from the space shuttle and is accelerated by means of a solid rocket motor toward Earth, so as to achieve atmospheric entry conditions close to those of a spacecraft returning from GEO. Following the atmospheric pass, the AFE spacecraft ascends to the specified LEO via an intermediate parking Earth orbit (PEO). The final maneuver includes the rendezvous with and the capture by the space shuttle. The entry and exit orbital planes of the AFE spacecraft are identical with the orbital plane of the space shuttle.

In this report, with reference to the AFE spacecraft, an actual GEO-to-LEO transfer is considered and optimal trajectories are determined by minimizing the total characteristic velocity. The optimization is performed with respect to the time history of the controls (angle of attack and angle of bank), the entry path inclination and the flight time being free. Two transfer maneuvers are considered: (DA) direct ascent to LEO; (IA) indirect ascent to LEO via PEO.

While the motion of the AFE spacecraft in a 3D-space is described by a system of six ODEs, substantial simplifications are possible if one exploits these facts: (i) the instantaneous orbital plane is nearly identical with the initial orbital plane;

(ii) the bank angle is small; and (iii) the Earth's angular velocity is relatively small. Under these assumptions, the complete system can be decoupled into two subsystems, one describing the longitudinal motion and one describing the lateral motion.

The angle of attack history, the entry path inclination, and the flight time are determined via the longitudinal motion subsystem; in this subsystem, the total characteristic velocity is minimized subject to the specified LEO requirement. The angle of bank history is determined via the lateral motion subsystem; in this subsystem, the difference between the instantaneous bank angle and a constant bank angle is minimized in the least square sense subject to the specified orbital inclination requirement.

It is shown that both the angle of attack and the angle of bank are constant. This result has considerable importance in the design of nominal trajectories to be used in the guidance of AFE and AOT vehicles.

Key Words. Flight mechanics, astrodynamics, hypervelocity flight, aeroassisted orbital transfer, aeroassisted flight experiment, optimal trajectories, guidance trajectories, decomposition techniques, longitudinal motion, lateral motion, sequential gradient-restoration algorithm, nonlinear two-point boundary-value problems.

Notations

C_D = drag coefficient;

C_L = lift coefficient;

C_{LP} = projected lift coefficient;

C_M = moment coefficient;

D = drag, N;

DP = dynamic pressure, N/m^2;

E = lift-to-drag ratio modulus;

g = local acceleration of gravity, m/sec^2;

h = altitude, m;

h_a = thickness of the atmosphere, m;

HR = heating rate, W/m^2;

i = orbital inclination, rad;

L = lift, N;

m = mass, kg;

r = radial distance from the center of the Earth, m;

r_e = radius of the Earth, m;

r_a = radius of the outer edge of the atmosphere, m;

S = reference surface area, m^2;

t = T/τ = dimensionless time;

T = running time, sec;

V = velocity, m/sec;

V_a = circular velocity at $r = r_a$, m/sec;

V_* = reference velocity, m/sec;

α = angle of attack, rad;

γ = path inclination, rad;

η = wedge angle, rad;

θ = longitude, rad;

μ = bank angle, rad;

μ_e = Earth's gravitational constant, m^3/sec^2;

ρ = air density, kg/m^3;

ρ_* = reference air density, kg/m^3;

τ = final time, sec;

ϕ = latitude, rad;

χ = heading angle, rad;

ω = angular velocity of the Earth, rad/sec;

Ω = longitude of the ascending node, rad;

ΔC_L = lift coefficient range;

ΔC_{LP}= projected lift coefficient range;

ΔV = characteristic velocity, m/sec.

Subscripts

0 = entry into the atmosphere;

1 = exit from the atmosphere;

00 = exit from the initial orbit;

11 = entry into the final orbit;

22 = entry into the parking orbit.

Superscripts

$\cdot$ = derivative with respect to dimensionless time;

$\sim$ = variable computed in an inertial system.

Acronyms

AFE = aeroassisted flight experiment;

AOT = aeroassisted orbital transfer;

DA = direct ascent;

DAOT = direct ascent optimal trajectory;

GEO = geosynchronous Earth orbit;

HEO = high Earth orbit;

IA = indirect ascent;

IAOT = indirect ascent optimal trajectory;

IART = indirect ascent reference trajectory;

LEO = low Earth orbit;

ODE = ordinary differential equation;

OT = optimal trajectory;

PEO = parking Earth orbit;

RT = reference trajectory;

SGRA = sequential gradient-restoration algorithm;

TPBVP = two-point boundary-value problem.

1. Introduction

The field of aeroassisted orbital transfer (AOT) has received considerable attention in recent years. For a spacecraft which must be transferred from a high Earth orbit (HEO) to a low Earth orbit (LEO), considerable savings in characteristic velocity are possible if the AOT mode is employed instead of the all-propulsive mode. In turn, this leads to propellant savings/payload increases.

In the all-propulsive mode or Hohmann transfer mode, the spacecraft navigates in the region between HEO and LEO. It must be braked propulsively twice, once to deorbit from HEO and once to achieve circularization into LEO.

In the AOT mode or synergistic mode, the spacecraft deorbits from HEO, undershoots LEO, enters the Earth's atmosphere, and uses the aerodynamic forces in order to deplete excess velocity. Then, after exiting the atmosphere, it reaches LEO with nearly-circular velocity. The resulting savings in propellant weight are beneficial; however, added thermal protection is needed to cope with the heating rates generated while the spacecraft traverses the upper atmosphere at hypervelocity speeds.

Aeroassisted orbital transfer is not only important for HEO-to-LEO transfer maneuvers, but may prove to be indispensable to future planetary flights. In particular, this statement refers to lunar return vehicles, Mars exploration vehicles, and Mars return vehicles. Indeed it is known that, for a round-trip

Earth-to-Mars mission, the total characteristic velocity of the AOT mode is about half that of the all-propulsive mode.

While the AOT prospects are clearly bright (Ref. 1), to take proper advantage of them it is necessary that guidance and control systems be designed with care. In turn, this requires the previous study of optimal trajectories, since they supply the ideal benchmark that guidance trajectories should strive to approach (Refs. 2-7).

1.1. Aeroassisted Flight Experiment. Because the AOT idea is yet untested, NASA has planned an aeroassisted flight experiment (AFE) involving a spacecraft to be launched and then recovered by the space shuttle (Refs. 8-9). The experiment simulates a transfer from a geosynchronous Earth orbit (GEO) to a low Earth orbit (LEO) and is tentatively scheduled for 1994. Specifically, the AFE spacecraft is released from the space shuttle and is accelerated by means of a solid rocket motor toward Earth, so as to achieve atmospheric entry conditions close to those of a spacecraft returning from GEO. During the atmospheric pass, aerodynamic/thermal data are gathered for use in designing AOT vehicles. Following the atmospheric pass, the AFE spacecraft ascends to the specified LEO via an intermediate parking Earth orbit (PEO). The final maneuver includes the rendezvous with and the capture by the space shuttle. Clearly,the entry and exit orbital planes of the AFE spacecraft are identical with the orbital plane of the space shuttle.

The configuration chosen for the AFE spacecraft is the so-called raked-cone configuration (Fig. 1), which is dominated by heating rate considerations rather than by aerodynamic performance considerations. Therefore, the lift-to-drag ratio modulus is very low, $E = 0.28$, at the design angle of attack, $\alpha = 17$ deg; also, the lift coefficient range is quite low, $-0.47 \leq C_L \leq -0.21$, in the angle of attack range $27 \geq \alpha \geq 7$ deg.

One way to solve the problems arising from the fact that $|\Delta C_L|$ is small, $|\Delta C_L| = 0.26$, is to fix the angle of attack at $\alpha = 17$ deg, corresponding to $C_L = -0.38$, and use the bank angle to control both the longitudinal motion and the lateral motion (Refs. 8-9). Let $L_P = L\cos\mu$ denote the vertical projection of the lift, and let $C_{LP} = C_L\cos\mu$ denote the projected lift coefficient. Because $-1 \leq \cos\mu \leq +1$, it is easy to see that $|\Delta C_{LP}| = 0.76$. Hence, the projected lift coefficient range is three times the lift coefficient range. To sum up, the control of the longitudinal motion is obtained by changing the modulus of the bank angle, while the control of the lateral motion is obtained by changing the sign of the bank angle. Reference 8 provides a nominal trajectory in which the bank angle history is represented by five constant-bank-angle segments and therefore involves four switches of the bank angle.

1.2. AFE Optimal Trajectories. Independently of the present plans for the aeroassisted flight experiment, it is of interest to determine the optimal trajectories of the AFE spacecraft. This study was carried out in Refs. 10-14 under the following assumptions: (a) the angle of attack is constant, $\alpha = 17$ deg;

(b) the spacecraft is controlled via the angle of bank; (c) the entry conditions are identical with those of the nominal trajectory of Ref. 8. In particular, in an inertial reference frame, the entry path inclination is fixed, $\tilde{\gamma}_0 = -4.49$ deg. From the extensive numerical computations, the following conclusions were obtained in Refs. 10-14:

(i) the optimal trajectories are two-subarc trajectories, with the bank angle constant in each subarc; hence, the control is bang-bang;

(ii) in the atmospheric entry phase, the bank angle is $\mu = 176.7$ deg, yielding a positive vertical component of the lift, which in turn helps the path inclination to increase gradually from the entry negative value to nearly zero value;

(iii) in the atmospheric exit phase, the bank angle is $\mu = 5.5$ deg, yielding a negative vertical component of the lift, which offsets the centrifugal force effects due to the curvature of the Earth, so as to ensure exit conditions compatible with the specified LEO;

(iv) the horizontal component of the lift during the atmospheric entry phase and the horizontal component of the lift during the atmospheric exit phase have the same sign and the same order of magnitude; they are directed in such a way that they nearly offset the effects due to the Earth's rotation; in this way, the instantaneous orbital plane is almost identical with the initial orbital plane, meaning that the wedge angle is nearly zero during the atmospheric pass; this means that, for efficient flight, the

motion of the AFE spacecraft is nearly planar in an inertial space; in other words, one must avoid energy dissipation associated with the lateral motion.

1.3. Present Research. This paper extends the optimization studies initiated in Ref. 10-14 to the case where (a) the AFE spacecraft is controlled via both the angle of attack and the angle of bank and (b) the entry conditions are identical with those of the nominal trajectory of Ref. 8, except the path inclination and the velocity, which are optimized. Optimal trajectories are studied for two transfer maneuvers: (DA) direct ascent to LEO; (IA) indirect ascent to LEO via PEO.

While the motion of the AFE spacecraft in a 3D-space is described by a system of six ODEs, substantial simplifications are possible if one exploits these facts: (i) the instantaneous orbital plane is nearly identical with the initial orbital plane; (ii) the bank angle is small; and (iii) the Earth's angular velocity is relatively small. Under these assumptions, the complete system can be decoupled into two subsystems, one describing the longitudinal motion and one describing the lateral motion.

The angle of attack history, the entry path inclination, and the flight time are determined via the longitudinal motion subsystem; in this subsystem, the total characteristic velocity is minimized subject to the specified LEO requirement. The angle of bank history is determined via the lateral motion subsystem; in this subsystem, the difference between the instantaneous bank

angle and a constant bank angle is minimized in the least square sense subject to the specified orbital inclination requirement.

It is shown that both the angle of attack and the angle of bank are constant. This result has considerable importance in the design of nominal trajectories to be used in the guidance of AFE and AOT vehicles.

1.4. Outline. Section 2 contains the system description, and Section 3 describes the optimal control problems to be solved. Section 4 introduces the decomposition technique, leading to the decoupling of the longitudinal motion (Section 5) from the lateral motion (Section 6). The experimental data are given in Section 7, and the numerical results are shown in Section 8. Finally, the conclusions are given in Section 9.

2. System Description

The motion of the AFE spacecraft takes place partly in space and partly in the atmosphere. For the purposes of this report, the trajectory begins at GEO (h = 19323 NM = 35786 km) and ends at LEO (h = 178 NM = 330 km). It includes a preatmospheric branch, an atmospheric branch, and a postatmospheric branch. Depending on the nature of the postatmospheric branch, we consider two transfer maneuvers:(DA) direct ascent to LEO; (IA) indirect ascent to LEO via an intermediate parking Earth orbit (PEO, h = 197 NM = 365 km). We assume that GEO, LEO, and PEO are circular orbits.

For Transfer (DA), the key points of the maneuver are these: point 00, exit from GEO; point 0, atmospheric entry; point 1, atmospheric exit; point 11, entry into LEO. Point 00 is the apogee of the preatmospheric transfer orbit 00 → 0; point 11 is the apogee of the postatmospheric transfer orbit 1 → 11. Propulsive impulses are applied at two points: at point 00 to deorbit from GEO; at point 11 in order to circularize the motion into LEO. See Fig. 2A.

For Transfer (IA), the key points of the maneuver are these: point 00, exit from GEO; point 0, atmospheric entry;point 1, atmospheric exit; point 22, entry into PEO; and point 11, entry into LEO. Point 00 is the apogee of the preatmospheric transfer orbit 00 → 0; point 22 is the apogee of both the first post-atmospheric transfer orbit 1 → 22 and the second postatmospheric transfer orbit 22 → 11; point 11 is the perigee of the second postatmospheric transfer orbit 22 → 11. Propulsive impulses are

applied at three points: at point 00 to deorbit from GEO; at point 22 in order to raise the height of the perigee of the second postatmospheric transfer orbit; and at point 11 in order to circularize the motion into LEO. See Fig. 2B.

For the atmospheric portion ($h \leq h_a$) of the trajectory of the AFE spacecraft, we employ an Earth-fixed system; for the space portion of the trajectory ($h > h_a$), we employ an inertial system; here, h_a = 400000 ft $\cong$ 122 km denotes the thickness of the atmosphere. For $h \leq h_a$, we compute the air density using the US Standard Atmosphere, 1976 (Ref. 15); for $h > h_a$, we assume that the air density is zero. For both the atmospheric portion and the space portions of the trajectory, we neglect the effects due to the oblateness of the Earth; we assume that the gravitational field is central and obeys the inverse square law.

2.1. Atmospheric Pass. With reference to the atmospheric portion of the trajectory of the AFE vehicle, the following additional hypotheses are employed: (a) the atmospheric pass is made with engine shut off; hence, the AFE spacecraft behaves as a particle of constant mass; (b) under extreme hypersonic conditions, the dependence of the aerodynamic coefficients on the Mach number and the Reynolds number is disregarded; (c) the sideslip angle is zero; hence, the side force component of the aerodynamic force is zero; (d) the AFE spacecraft is controlled

via the angle of attack and the angle of bank.

2.2. Differential System. With the above assumptions, upon using an Earth-fixed system, and upon normalizing the interval of integration to unity, the equations of motion include the kinematical equations (Ref. 10)

$$\dot{\theta} = \tau(V\cos\gamma\ \cos\chi/r\cos\phi), \tag{1a}$$

$$\dot{\phi} = \tau(-V\cos\gamma\ \sin\chi/r), \tag{1b}$$

$$\dot{r} = \tau(V\sin\gamma), \tag{1c}$$

and the dynamical equations (Ref. 10)

$$\dot{V} = \tau(-D/m - g\sin\gamma) + \tau[\omega^2 r(\sin\gamma\ \cos^2\phi + \cos\gamma\ \sin\chi\ \cos\phi\ \sin\phi)], \tag{2a}$$

$$\dot{\gamma} = \tau[(L/mV)\cos\mu + (V/r - g/V)\cos\gamma + 2\omega\ \cos\chi\ \cos\phi] + \tau[(\omega^2 r/V)(\cos\gamma\ \cos^2\phi - \sin\gamma\ \sin\chi\ \cos\phi\ \sin\phi)], \tag{2b}$$

$$\dot{\chi} = \tau[(L/mV)\sin\mu/\cos\gamma + (V/r)\cos\gamma\ \cos\chi\ \tan\phi] + \tau[2\omega(\sin\phi + \tan\gamma\ \sin\chi\ \cos\phi)] + \tau[(\omega^2 r/V)\cos\chi\ \cos\phi\ \sin\phi/\cos\gamma]. \tag{2c}$$

In the dynamical equations, the symbol ω denotes the angular velocity of the Earth; terms linear in ω are due to the Coriolis acceleration; terms quadratic in ω are due to the transport acceleration. Also in the dynamical equations, the local acceleration of gravity is given by

$$g = \mu_e/r^2, \tag{3}$$

where μ_e denotes the Earth's gravitational constant. In addition, the aerodynamic forces are given by

$$D = (1/2)C_D(\alpha)\rho(h)SV^2, \tag{4a}$$

$$L = (1/2)C_L(\alpha)\rho(h)SV^2, \tag{4b}$$

where the air density ρ depends on the altitude h, with

$$h = r - r_e. \tag{4c}$$

For given initial conditions, parameter τ, and controls $\alpha(t)$ and $\mu(t)$, Eqs. (1)-(4) can be integrated in forward time over the time interval $0 \leq t \leq 1$. Here, the initial time $t = 0$ corresponds to atmospheric entry and the final time $t = 1$ corresponds to atmospheric exit.

2.3. Control Constraint. To obtain realistic solutions, the presence of upper and lower bounds on the angle of attack is necessary. Therefore, the two-sided inequality constraint

$$\alpha_L \leq \alpha \leq \alpha_U, \qquad 0 \leq t \leq 1, \tag{5}$$

must be satisfied everywhere along the interval of integration.

2.4. Transformation Relations. General transformation relations allow one to pass from quantities computed in an Earth-fixed system to quantities computed in an inertial system (direct relations), and viceversa (inverse relations). See Refs.10-11 for details.

For the kinematic variables, the direct relations are

$$\tilde{\theta} = \theta + \tau\omega t, \tag{6a}$$

$$\tilde{\phi} = \phi, \tag{6b}$$

$$\tilde{r} = r, \tag{6c}$$

and the inverse relations are

$$\theta = \tilde{\theta} - \tau\omega t, \tag{7a}$$

$$\phi = \tilde{\phi}, \tag{7b}$$

$$r = \tilde{r}. \tag{7c}$$

For the dynamic variables, the general transformation relations are

$$\tilde{V}\cos\tilde{\gamma}\cos\tilde{\chi} = V\cos\gamma\cos\chi + \omega r\cos\phi, \tag{8a}$$

$$\tilde{V}\cos\tilde{\gamma}\sin\tilde{\chi} = V\cos\gamma\sin\chi, \tag{8b}$$

$$\tilde{V}\sin\tilde{\gamma} = V\sin\gamma, \tag{8c}$$

and they imply the direct relations

$$\tilde{V} = \sqrt{[V^2 + 2\omega rV\cos\gamma\cos\chi\cos\phi + (\omega r\cos\phi)^2]}, \tag{9a}$$

$$\tan\tilde{\gamma} = V\sin\gamma/\sqrt{[(V\cos\gamma)^2 + 2\omega rV\cos\gamma\cos\chi\cos\phi + (\omega r\cos\phi)^2]}, \tag{9b}$$

$$\tan\tilde{\chi} = V\cos\gamma\sin\chi/(V\cos\gamma\cos\chi + \omega r\cos\phi), \tag{9c}$$

and the inverse relations

$$V = \sqrt{[\tilde{V}^2 - 2\omega\tilde{r}\tilde{V}\cos\tilde{\gamma}\cos\tilde{\chi}\cos\tilde{\phi} + (\omega\tilde{r}\cos\tilde{\phi})^2]}, \quad (10a)$$

$$\tan\gamma = \tilde{V}\sin\tilde{\gamma}/\sqrt{[(\tilde{V}\cos\tilde{\gamma})^2 - 2\omega\tilde{r}\tilde{V}\cos\tilde{\gamma}\cos\tilde{\chi}\cos\tilde{\phi} + (\omega\tilde{r}\cos\tilde{\phi})^2]}, \quad (10b)$$

$$\tan\chi = \tilde{V}\cos\tilde{\gamma}\sin\tilde{\chi}/(\tilde{V}\cos\tilde{\gamma}\cos\tilde{\chi} - \omega\tilde{r}\cos\tilde{\phi}). \quad (10c)$$

If the Earth's rotation is neglected ($\omega = 0$), the inertial quantities appearing in Eqs.(6)-(10) become identical to the corresponding Earth-fixed quantities. However, this is not the case if the Earth's rotation is considered ($\omega \neq 0$).

2.5. Orbital Elements. Once the state variables are known, one can compute some important quantities such as the orbital inclination, the longitude of the ascending node, and the wedge angle; the latter is the angle between the instantaneous orbital plane and the entry orbital plane. In the inertial system, these quantities are defined through the relations

$$\cos\tilde{i} = \cos\tilde{\phi}\cos\tilde{\chi}, \quad (11a)$$

$$\sin(\tilde{\theta} - \tilde{\Omega}) = \cot\tilde{i}\tan\tilde{\phi}, \quad (11b)$$

$$\cos\tilde{\eta} = \sin\tilde{i}\sin\tilde{i}_0\cos(\tilde{\Omega} - \tilde{\Omega}_0) + \cos\tilde{i}\cos\tilde{i}_0. \quad (11c)$$

In the Earth-fixed system, the relations analogous to (11) are defined below:

$$\cos i = \cos\phi\cos\chi, \quad (12a)$$

$$\sin(\theta - \Omega) = \cot i\tan\phi, \quad (12b)$$

$$\cos\eta = \sin i\sin i_0\cos(\Omega - \Omega_0) + \cos i\cos i_0. \quad (12c)$$

If the Earth's rotation is neglected ($\omega = 0$), the inertial quantities appearing in Eqs. (11) become identical to the corresponding Earth-fixed quantities. However, this is not the case if the Earth's rotation is considered ($\omega \neq 0$).

2.6. Initial Conditions. At atmospheric entry, the initial values of the state variables $\tilde{\theta}_0$, $\tilde{\phi}_0$, $\tilde{r}_0$, $\tilde{\chi}_0$ are given in the inertial system. In particular,

$$\tilde{r}_0 = r_a. \tag{13a}$$

Because of the relations (11), the initial values of the orbital elements $\tilde{i}_0$, $\tilde{\Omega}_0$, $\tilde{\eta}_0$ are known. In particular,

$$\tilde{\eta}_0 = 0, \tag{13b}$$

by definition. The initial values of the state variables $\tilde{V}_0$, $\tilde{\gamma}_0$ must be consistent with the relation

$$r_{00}^2(2V_*^2 - \tilde{V}_0^2) - 2r_{00}r_a V_*^2 + r_a^2\tilde{V}_0^2\cos^2\tilde{\gamma}_0 = 0, \tag{13c}$$

where $V_* = \tilde{V}_a = \sqrt{(\mu_e/r_a)} = 7.831$ km/sec is a reference velocity, i.e., the circular velocity at $r = r_a$. This relation arises from energy conservation and angular momentum conservation applied to the preatmospheric transfer orbit $00 \rightarrow 0$ connecting GEO with atmospheric entry.

2.7. Final Conditions. At atmospheric exit, the final time τ is free and must be determined in such a way that

$$\tilde{r}_1 = r_a. \tag{14a}$$

The final values of the state variables $\tilde{\theta}_1$, $\tilde{\phi}_1$, $\tilde{\chi}_1$ must be consistent with the relation

$$\tilde{\eta}_1 = 0. \tag{14b}$$

This means that the final value of the wedge angle must vanish, hence that the exit orbital plane must be identical with the entry orbital plane. The final values of the state variables $\tilde{V}_1$, $\tilde{\gamma}_1$ must be consistent with either the relation

$$\text{(DA)} \quad r_{11}^2(2V_*^2 - \tilde{V}_1^2) - 2r_{11}r_a V_*^2 + r_a^2\tilde{V}_1^2\cos^2\tilde{\gamma}_1 = 0 \tag{14c}$$

or the relation

$$\text{(IA)} \quad r_{22}^2(2V_*^2 - \tilde{V}_1^2) - 2r_{22}r_a V_*^2 + r_a^2\tilde{V}_1^2\cos^2\tilde{\gamma}_1 = 0. \tag{14d}$$

Equation (14c) refers to the direct ascent case and arises from energy conservation and angular momentum conservation applied to the postatmospheric transfer orbit 1 → 11 connecting atmospheric exit with LEO. Equation (14d) refers to the indirect ascent case and arises from energy conservation and angular momentum conservation applied to the postatmospheric transfer orbit 1 → 22 connecting atmospheric exit with PEO.

2.8. Summary. The relations governing the atmospheric pass include the differential system (1)-(4), the control constraint (5), and the boundary conditions (13)-(14). In the boundary conditions, the inertial quantities are related to the Earth-fixed quantities via the transformation relations (6)-(10); also, the inertial quantities are related to the orbital elements via the trigonometric relations (11). In this formulation, the independent variable is the time t, $0 \leq t \leq 1$. The dependent variables include six state variables [$\theta(t)$, $\phi(t)$, $r(t)$, $V(t)$, $\gamma(t)$, $\chi(t)$], two control variables [$\alpha(t)$, $\mu(t)$], and one parameter (τ).

3. Optimal Control Problems

Subject to the previous constraints, different optimal control problems can be formulated, depending on the performance index chosen and the type of transfer maneuver considered. Here, we focus attention on the minimization of the total characteristic velocity $\Delta\tilde{V}$, which is a measure of the propellant required for orbital transfer.

Problem (DA). This problem refers to the direct ascent to LEO. The functional to be minimized is given by

$$I = \Delta\tilde{V} = \Delta\tilde{V}_{00} + \Delta\tilde{V}_{11}, \tag{15a}$$

with

$$\Delta\tilde{V}_{00} = \sqrt{(r_a/r_{00})}V_* - (r_a/r_{00})\tilde{V}_0\cos\tilde{\gamma}_0, \tag{15b}$$

$$\Delta\tilde{V}_{11} = \sqrt{(r_a/r_{11})}V_* - (r_a/r_{11})\tilde{V}_1\cos\tilde{\gamma}_1. \tag{15c}$$

Problem (IA). This problem refers to the indirect ascent to LEO via PEO. The functional to be minimized is given by

$$I = \Delta\tilde{V} = \Delta\tilde{V}_{00} + \Delta\tilde{V}_{22} + \Delta\tilde{V}_{11}, \tag{16a}$$

with

$$\Delta\tilde{V}_{00} = \sqrt{(r_a/r_{00})}V_* - (r_a/r_{00})\tilde{V}_0\cos\tilde{\gamma}_0, \tag{16b}$$

$$\Delta\tilde{V}_{22} = \sqrt{[2r_a r_{11}/(r_{11}r_{22} + r_{22}^2)]}V_* - (r_a/r_{22})\tilde{V}_1\cos\tilde{\gamma}_1, \tag{16c}$$

$$\Delta\tilde{V}_{11} = \sqrt{[2r_a r_{22}/(r_{11}r_{22} + r_{11}^2)]}V_* - \sqrt{(r_a/r_{11})}V_*. \tag{16d}$$

4. Decomposition Technique

The study of the optimal trajectories of an AFE vehicle can be simplified to a considerable degree if the complete system of differential equations, inequality constraints, and boundary conditions can be decomposed into a subsystem governing the longitudinal motion [state variables $r(t)$, $V(t)$, $\gamma(t)$; control variable $\alpha(t)$; unknown parameter τ] and a subsystem governing the lateral motion [state variables $\theta(t)$, $\phi(t)$, $\chi(t)$; control variable $\mu(t)$; known parameter τ]. The decomposition is possible if the following approximations are introduced into the equations of motion:

$$i \cong i_0, \tag{17a}$$

$$\mu^2 << 1, \tag{17b}$$

$$\omega^2 \cong 0. \tag{17c}$$

Approximation (17a) means that the instantaneous orbital plane is nearly identical with the initial orbital plane. Approximation (17b) means that the bank angle is small. Approximation (17c) means that terms quadratic in ω are small with respect to terms linear in ω and terms not containing ω. The following relations arise as a consequence of the approximations (17):

$$\cos i_0 \cong \cos\phi \cos\chi, \tag{18a}$$

$$\cos\mu \cong 1, \tag{18b}$$

$$\tilde{V} \cong \sqrt{[V^2 + 2\omega r V \cos\gamma \cos i_0]}, \tag{18c}$$

$$\tilde{V}\cos\tilde{\gamma} \cong \sqrt{[V^2\cos^2\gamma + 2\omega r V \cos\gamma \cos i_0]}. \tag{18d}$$

Relation (18a) is due to (12a) and (17a). Relation (18b) is a restatement of (17b). Relation (18c) is obtained by combining (9a), (17c),and (18a). Relation (18d) arises from (8a), (8b), (17c),and (18a). As the subsequent analysis shows, the approximations (17) and the implications (18) are essential to a simplified study of the longitudinal motion (Section 5), but nonessential, hence optional, to a simplified study of the lateral motion (Section 6).

5. Longitudinal Motion

In the Earth-fixed system, the subsystem governing the longitudinal motion includes the differential equations

$$\dot{r} = \tau[V\sin\gamma], \tag{19a}$$

$$\dot{V} = \tau[-D/m - g\sin\gamma], \tag{19b}$$

$$\dot{\gamma} = \tau[L/mV + (V/r - g/V)\cos\gamma + 2\omega\cos i_0], \tag{19c}$$

the control inequality constraint

$$\alpha_L \leq \alpha \leq \alpha_U, \tag{20}$$

the initial conditions

$$r_0 = r_a, \tag{21a}$$

$$2V_*^2(r_{00}^2 - r_{00}r_a) + 2\omega r_a V_0 \cos\gamma_0 \cos i_0 (r_a^2 - r_{00}^2) + V_0^2(r_a^2\cos^2\gamma_0 - r_{00}^2) = 0, \tag{21b}$$

the final conditions

$$r_1 = r_a \tag{22a}$$

and either

$$\text{(DA)}\quad 2V_*^2(r_{11}^2 - r_{11}r_a) + 2\omega r_a V_1 \cos\gamma_1 \cos i_0 (r_a^2 - r_{11}^2) + V_1^2(r_a^2\cos^2\gamma_1 - r_{11}^2) = 0, \tag{22b}$$

or

$$\text{(IA)}\quad 2V_*^2(r_{22}^2 - r_{22}r_a) + 2\omega r_a V_1 \cos\gamma_1 \cos i_0 (r_a^2 - r_{22}^2) + V_1^2(r_a^2\cos^2\gamma_1 - r_{22}^2) = 0. \tag{22c}$$

Relations (19)-(22) are obtained from (1c), (2a), (2b), (5), (13a), (13c), (14a), (14c), (14d) after accounting for (6), (8), the approximations (17), and the implications (18).

5.1. Performance Indexes. Using (17)-(18), the performance indexes of the optimal control problems of Section 3 can be reformulated below. For the direct ascent to LEO, Eqs. (15) become

$$\text{(DA)}\quad I = \Delta\tilde{V} = \Delta\tilde{V}_{00} + \Delta\tilde{V}_{11}, \tag{23a}$$

with

$$\Delta\tilde{V}_{00} = \sqrt{(r_a/r_{00})}V_* - (r_a/r_{00})\sqrt{(V_0^2\cos^2\gamma_0 + 2\omega r_a V_0 \cos\gamma_0 \cos i_0)}, \tag{23b}$$

$$\Delta\tilde{V}_{11} = \sqrt{(r_a/r_{11})}V_* - (r_a/r_{11})\sqrt{(V_1^2\cos^2\gamma_1 + 2\omega r_a V_1 \cos\gamma_1 \cos i_0)}. \tag{23c}$$

For the indirect ascent to LEO via PEO, Eqs. (16) become

$$\text{(IA)}\quad I = \Delta\tilde{V} = \Delta\tilde{V}_{00} + \Delta\tilde{V}_{22} + \Delta\tilde{V}_{11}, \tag{24a}$$

with

$$\Delta\tilde{V}_{00} = \sqrt{(r_a/r_{00})}V_* - (r_a/r_{00})\sqrt{(V_0^2\cos^2\gamma_0 + 2\omega r_a V_0 \cos\gamma_0 \cos i_0)}, \tag{24b}$$

$$\Delta\tilde{V}_{22} = \sqrt{[2r_a r_{11}/(r_{11}r_{22} + r_{22}^2)]}V_* - (r_a/r_{22})\sqrt{(V_1^2\cos^2\gamma_1 + 2\omega r_a V_1 \cos\gamma_1 \cos i_0)}, \quad (24c)$$

$$\Delta\tilde{V}_{11} = \sqrt{[2r_a r_{22}/(r_{11}r_{22} + r_{11}^2)]}V_* - \sqrt{(r_a/r_{11})}V_*. \quad (24d)$$

5.2. Summary. The relations governing the longitudinal motion include the differential system (19), the control constraint (20), and the boundary conditions (21)-(22). In this formulation, the independent variable is the time t, $0 \leq t \leq 1$. The dependent variables include three state variables [r(t), V(t), γ(t)], one control variable [α(t)], and one parameter (τ). These variables must be determined in such a way that the performance index (23) is minimized in the direct ascent case and the performance index (24) is minimized in the indirect ascent case.

6. Lateral Motion

In the Earth-fixed system, the subsystem governing the lateral motion includes the differential equations

$$\dot{\theta} = \tau(V\cos\gamma\ \cos\chi/r\cos\phi), \tag{25a}$$

$$\dot{\phi} = \tau(-V\cos\gamma\ \sin\chi/r), \tag{25b}$$

$$\begin{aligned}\dot{\chi} = {} & \tau[(L/mV)\sin\mu/\cos\gamma + (V/r)\cos\gamma\ \cos\chi\ \tan\phi] \\ & + \tau[2\omega(\sin\phi + \tan\gamma\ \sin\chi\ \cos\phi)] \\ & + \tau[(\omega^2 r/V)\cos\chi\ \cos\phi\ \sin\phi/\cos\gamma],\end{aligned} \tag{25c}$$

the initial conditions

$$\theta_0 = \text{given}, \tag{26a}$$

$$\phi_0 = \text{given}, \tag{26b}$$

$$\chi_0 = \text{given}, \tag{26c}$$

and the final condition

$$\tilde{\eta}_1 = 0. \tag{27a}$$

It must be noted that the functions $r(t)$, $V(t)$, $\gamma(t)$, $\alpha(t)$, τ are known from the solution of the optimization problem associated with the longitudinal motion (Section 5). It must also be noted that, on account of the definitions (11) and the transformation relations (6) and (9), the final condition (27a) can be rewritten in the functional form

$$\tilde{\eta}_1(\theta_1, \phi_1, \chi_1) = 0, \tag{27b}$$

which replaces (27a).

6.1. Performance Index. In the subsystem (25)-(27), the dependent variables include three state variables [$\theta(t)$, $\phi(t)$, $\chi(t)$] and one control variable [$\mu(t)$]. There is no parameter, since τ is known. Therefore, the subsystem (25)-(27) admits an infinite number of solutions for the bank angle $\mu(t)$. The solution can be rendered unique by requiring that an optimization criterion be met, such as minimizing the functional

$$I = \int_0^1 (\mu - \pi)^2 dt, \tag{28}$$

where π is a parameter. The solution of the optimal control problem (25)-(28) has the form

$$\mu(t) = \pi = \text{const.} \tag{29}$$

Indeed, it can be readily shown that the multipliers associated with the constraints (25)-(27) all vanish.

6.2. Two-Point Boundary-Value Problem. For the purposes of explanation, observe that (29) implies that

$$\dot{\mu} = 0. \tag{30}$$

Then, the subsystem (25)-(27) augmented by (30) constitutes a two-point boundary-value problem (TPBVP) in which the unknowns are the functions $\theta(t)$, $\phi(t)$, $\chi(t)$, $\mu(t)$. Since there are four differential equations and four boundary conditions, one surmises that a solution might exist; however, because the TPBVP (25)-(27)

and (30) is nonlinear, the existence of a solution must be confirmed by numerical tests.

6.3. Remark. While the hypothesis (17c) is essential to a simplified study of the longitudinal motion, it is optional to a simplified study of the lateral motion. Indeed, the previous considerations stand unchanged regardless of whether the ω^2 term is dropped or retained in (25c). If it is retained, then a slightly more precise solution is obtained for the lateral motion.

7. Experimental Data

The following data were used in the numerical experiments.

Spacecraft Data. The AFE configuration is shown in Fig. 1. The mass of the AFE spacecraft is m = 1678 kg; the reference surface area is S = 14.31 m^2. For this configuration, the drag coefficient $C_D = C_D(\alpha)$ is shown in Fig. 3A, the lift coefficient $C_L = C_L(\alpha)$ is shown in Fig. 3B, the lift-to-drag ratio modulus $E = E(\alpha)$ is shown in Fig. 3C, and the drag polar $C_D = C_D(C_L)$ is shown in Fig. 3D. See also Table 1.

The functions appearing in Fig. 3 can be approximated by the relations

$$C_D = A_0 + A_1\alpha + A_2\alpha^2, \tag{31a}$$

$$C_L = B_0 + B_1\alpha + B_2\alpha^2, \tag{31b}$$

$$E = C_0 + C_1\alpha + C_2\alpha^2, \tag{31c}$$

$$C_D = D_0 + D_1C_L + D_2C_L^2, \tag{31d}$$

with

$$A_0 = 1.565, \quad A_1 = -0.306, \quad A_2 = -1.375, \tag{32a}$$

$$B_0 = -0.036, \quad B_1 = -1.557, \quad B_2 = 1.344, \tag{32b}$$

$$C_0 = 0.036, \quad C_1 = 0.836, \quad C_2 = -0.041, \tag{32c}$$

$$D_0 = 1.235, \quad D_1 = -2.379, \quad D_2 = -5.473. \tag{32d}$$

The angle of attack is subject to Ineq. (5),

$$\alpha_L \leq \alpha \leq \alpha_U, \tag{33a}$$

corresponding to

$$C_{LL} \leq C_L \leq C_{LU}. \tag{33b}$$

Note that the lower bound in (33a) corresponds to the upper bound in (33b), and viceversa. This is due to the fact that, because of the raked-cone configuration of the AFE spacecraft, the lift coefficient is a decreasing function of the angle of attack (see Fig. 3B).

In the numerical experiments, three alternative angle of attack ranges were considered, hence three alternative lift coefficient ranges were considered,through the following choices:

$$\text{(i)} \quad \alpha_L = 7.0 \text{ deg}, \quad \alpha_U = 27.0 \text{ deg}, \tag{34a}$$

$$\text{(ii)} \quad \alpha_L = 7.0 \text{ deg}, \quad \alpha_U = 17.0 \text{ deg}, \tag{34b}$$

$$\text{(iii)} \quad \alpha_L = 7.0 \text{ deg}, \quad \alpha_U = 10.0 \text{ deg}, \tag{34c}$$

corresponding to

$$\text{(i)} \quad C_{LL} = -0.47, \quad C_{LU} = -0.21, \tag{35a}$$

$$\text{(ii)} \quad C_{LL} = -0.38, \quad C_{LU} = -0.21, \tag{35b}$$

$$\text{(iii)} \quad C_{LL} = -0.27, \quad C_{LU} = -0.21. \tag{35c}$$

For these cases, the values of the maximum lift-to-drag ratio modulus are

(i) $E_{max} = 0.42,$ (36a)

(ii) $E_{max} = 0.28,$ (36b)

(iii) $E_{max} = 0.18,$ (36c)

and occur for $C_L = C_{LL}$.

Physical Constants. The radius of the Earth is r_e = 6378 km; the radius of the outer edge of the atmosphere is r_a = 6500 km; the thickness of the atmosphere is h_a = 122 km; the Earth's gravitational constant is μ_e = 0.3986E+06 km^3/sec^2; the circular velocity at $r = r_a$ is $\tilde{V}_a$ = 7.831 km/sec; the angular velocity of the Earth is ω = 0.7292E-04 rad/sec.

Atmospheric Model. The assumed atmospheric model is that of the US Standard Atmosphere, 1976 (Ref. 15). In this model, the values of the density are tabulated at discrete altitudes. For intermediate altitudes, the density is computed by assuming an exponential fit for the function $\rho(h)$.

Dynamic Pressure. The dynamic pressure is computed with the formula

$$DP = (1/2)\rho V^2. \quad (37a)$$

Heating Rate. The stagnation point heating rate is computed with the formula

$$HR = C\sqrt{(\rho/\rho_*)}(V/V_*)^{3.07}. \quad (37b)$$

Here, $\rho_* = 0.3097E\text{-}03$ kg/m^3 is a reference density, the density at $h_* = 60$ km; $V_* = \tilde{V}_a = 7.831$ km/sec is a reference velocity; the constant $C = 282.3$ W/cm^2 represents the stagnation point heating rate at $\rho = \rho_*$ and $V = V_*$, based on a nose radius of one foot.

Atmospheric Entry. In the inertial system, the given initial conditions are as follows: the longitude is $\tilde{\theta}_0 = -134.52$ deg; the latitude is $\tilde{\phi}_0 = -4.49$ deg; the altitude is $h_0 = 122$ km, corresponding to the radius $\tilde{r}_0 = 6500$ km; the heading angle is $\tilde{\chi}_0 = -28.13$ deg. The orbital inclination is $\tilde{i}_0 = 28.45$ deg; the longitude of the ascending node is $\tilde{\Omega}_0 = -126.19$ deg; the wedge angle is $\tilde{\eta}_0 = 0.00$ deg.

Atmospheric Exit. In the inertial system, the desired final conditions are as follows: the altitude is $h_1 = 122$ km, corresponding to the radius $\tilde{r}_1 = 6500$ km; the orbital inclination is $\tilde{i}_1 = 28.45$ deg; the longitude of the ascending node is $\tilde{\Omega}_1 = -126.19$ deg; the wedge angle is $\tilde{\eta}_1 = 0.00$ deg.

Transfer (DA). This is the direct ascent to LEO. The GEO conditions are as follows: the altitude is $h_{00} = 35786$ km, corresponding to the radius $\tilde{r}_{00} = 42164$ km; the path inclination is $\tilde{\gamma}_{00} = 0.00$ deg. The LEO conditions are as follows: the altitude is $h_{11} = 330$ km, corresponding to the radius $\tilde{r}_{11} = 6708$ km; the path inclination is $\tilde{\gamma}_{11} = 0.00$ deg.

Transfer (IA). This is the indirect ascent to LEO via PEO. The GEO conditions are as follows: the altitude is h_{00} = 35786 km, corresponding to the radius $\tilde{r}_{00}$ = 42164 km; the path inclination is $\tilde{\gamma}_{00}$ = 0.00 deg. The PEO conditions are as follows: the altitude is h_{22} = 365 km, corresponding to the radius $\tilde{r}_{22}$ = 6743 km; the path inclination is $\tilde{\gamma}_{22}$ = 0.00 deg. The LEO conditions are as follows: the altitude is h_{11} = 330 km, corresponding to the radius $\tilde{r}_{11}$ = 6708 km; the path inclination is $\tilde{\gamma}_{11}$ = 0.00 deg.

8. Numerical Results

The decomposition technique of Sections 4-6 was implemented for the AFE spacecraft in connection with the experimental data of Section 7. First, the longitudinal motion subsystem was solved with respect to the functions $r(t)$, $V(t)$, $\gamma(t)$, $\alpha(t)$ and the parameter τ which minimize the total characteristic velocity, while satisfying the desired LEO requirement; here, the sequential gradient-restoration algorithm (SGRA, see Refs. 16-18 for recent versions) was employed. Then, with the above functions and parameter fixed, the lateral motion subsystem was solved with respect to the functions $\theta(t)$, $\phi(t)$, $\chi(t)$, $\mu(t)$ which minimize the difference $\mu(t) - \pi$ in the least square sense, π being a parameter. This leads to a nonlinear two-point boundary-value problem (TPBVP); here, the modified quasilinearization algorithm was employed in conjunction with the method of particular solutions (MQA/MPS, see Refs. 19-21).

8.1. Effect of the Control Bounds. First, (DA) the direct ascent to LEO was considered, and optimal trajectories (OT) were computed for three alternative angle of attack ranges, corresponding to three alternative lift coefficient ranges, described by (33)-(36). In each case, consistently with the results of Ref. 7, it was found that optimality in the longitudinal motion is achieved by flying at the lift coefficient lower bound, hence at the angle of attack upper bound. Concerning the lateral motion, the least square deviation of the bank angle from a constant value is achieved by flying at constant bank angle.

Summary results can be found in Table 2, which shows the following quantities for DAOT Cases (i), (ii), (iii): the number of bank angle switches, the flight time, the angle of attack, the lift coefficient, and the angle of bank; the minimum altitude, the peak dynamic pressure, and the peak heating rate; the entry path inclination, the peak change of orbital inclination, the peak change of longitude of the ascending node, and the peak wedge angle; the characteristic velocity components and the total characteristic velocity.

As can be seen, the total characteristic velocities of DAOT Cases (i), (ii), (iii) are nearly the same. With respect to the characteristic velocity of Case (ii), that of Case (i) is 0.1% lower, while that of Case (iii) is 0.2% higher. However, the solution (ii) is to be preferred because of the following consideration: it is characterized by $C_M = 0$, where C_M is the moment coefficient (Ref. 8), while this is not the case with solutions (i) and (iii).

Comparison of DAOT Case (ii) with the DAOT solution presented in Ref. 14 shows that the entry path inclination is now flatter (by 0.36 deg). Consequently, the minimum altitude is higher (by about 0.6 km); hence, the peak dynamic pressure and the peak heating rate are lower than the corresponding quantities in Ref. 14.

8.2. Comparison of AFE Trajectories. Based on the results of the previous section, we restrict the analysis to Case (ii), namely the case where Ineqs. (33) have the form

$$\text{(ii)} \quad 7.0 \leq \alpha \leq 17.0 \text{ deg}, \tag{38a}$$

$$\text{(ii)} \quad -0.38 \leq C_L \leq -0.21. \tag{38b}$$

Both (DA) the direct ascent to LEO and (IA) the indirect ascent to LEO via PEO were considered, and optimal trajectories (OT) were computed. Once more, it was found that optimality in the longitudinal motion is achieved by flying at the upper bound angle of attack, hence at the lower bound lift coefficient. Concerning the lateral motion, optimality is achieved by flying at constant bank angle.

For comparison purposes and for (IA) the indirect ascent to LEO via PEO, a reference trajectory (RT) was also computed. This is the nominal trajectory of Ref. 8, which is flown at $\alpha = 17.0$ deg using $N_s = 4$ switches of the bank angle, hence $N = 5$ constant values of the bank angle, specifically:

$$\mu_1 = -180.0, \ \mu_2 = -43.9, \ \mu_3 = 89.9, \ \mu_4 = -89.9, \ \mu_5 = 0.0 \text{ deg}. \tag{39}$$

For trajectories DAOT, IAOT, and IART, Table 3 shows the following quantities: the number of bank angle switches, the flight time, the angle of attack, the lift coefficient, and the angle of bank; the minimum altitude, the peak dynamic pressure, and the peak heating rate; the entry path inclination, the peak change of orbital inclination, the peak change of longitude of the ascending node, and the peak wedge angle; the characteristic velocity components and the total characteristic velocity.

For trajectories DAOT, IAOT, and IART, and for both the Earth-fixed system and the inertial system, Tables 4-5 show the entry values (Table 4) and the exit values (Table 5) of the following quantities: longitude, latitude, altitude, radius, velocity, path inclination, and heading angle; orbital inclination, longitude of the ascending node, and wedge angle.

For trajectories DAOT, IAOT, and IART, Fig. 4 shows the time histories of the following quantities: relative longitude (Fig. 4A), latitude (Fig. 4B), altitude (Fig. 4C), relative velocity (Fig. 4D), relative path inclination (Fig. 4E), relative heading angle (Fig. 4F); angle of attack (Fig. 4G), lift coefficient (Fig. 4H), bank angle (Fig. 4I); dynamic pressure (Fig. 4J), heating rate (Fig. 4K); inertial orbital inclination (Fig. 4L), inertial longitude of the ascending node (Fig. 4M), and inertial wedge angle (Fig. 4N).

From Tables 3-5 and Fig. 4, the following comments arise:

(a) The total characteristic velocity of trajectory DAOT is less than that of trajectory IAOT, which in turn is less than that of trajectory IART.

(b) Compared with trajectory IART, trajectories DAOT and IAOT are characterized by flatter entry (by 0.36 deg), hence higher minimum altitude (by 3.3 km), lower peak dynamic pressure, lower peak heating rate, and longer flight time.

(c) The longer flight time of trajectories DAOT and IAOT vis-a-vis trajectory IART can be explained as follows: while

the velocity depletion $V_0 - V_1$ is about the same for the three trajectories, the first two are flown at higher altitude, hence smaller air density, hence less aerodynamic drag.

(d) Compared with trajectory IART, trajectories DAOT and IAOT involve much smaller values of the peak change of orbital inclination, peak change of longitude of the ascending node, and peak wedge angle. Indeed, for trajectories DAOT and IAOT, these quantities are nearly zero, within 1/100 deg. On the other hand, for trajectory IART, $\max|\Delta\tilde{i}| = 1.08$deg, $\max|\Delta\tilde{\Omega}| = 0.31$ deg, $\max(\tilde{\eta}) = 1.08$ deg.

8.3. Control Considerations. Trajectories DAOT, IAOT, and IART are all flown at the same angle of attack $\alpha = 17.0$ deg, hence at the same lift coefficient $C_L = -0.38$. This being the case, the control margin for the angle of attack, hence the control margin for the lift coefficient, is the same for the three trajectories.

Concerning the angle of bank, trajectories DAOT and IAOT are flown with $\mu = 5.14$ deg, while trajectory IART is flown with five subsequent values of the bank angle [see (39)]. Hence, trajectories DAOT and IAOT have a larger control margin for the angle of bank than trajectory IART.

It should be pointed out that trajectories DAOT, IAOT, and IART are inherently unstable if flown open-loop. For example, suppose that, at time instant t, there is a positive difference between the flight velocity and the nominal velocity. The higher flight velocity yields a higher centrifugal force

due to the Earth's curvature, hence a higher value of $\dot{\gamma}$, hence a higher altitude, hence a lower density, hence a lower drag, hence less velocity decrease vis-a-vis the nominal trajectory. Therefore, at time instant $t + \Delta t$, the positive difference between the flight velocity and the nominal trajectory has further increased, and so on. To sum up, (i) guidance and control systems must be designed with care; and (ii) feedback control schemes must be developed to ensure the stability of the AFE trajectory.

9. Conclusions

In this report,the GEO-to-LEO transfer of an AFE spacecraft is considered, and optimal trajectories are determined by minimizing the total characteristic velocity. The optimization is performed with respect to the time history of the controls (angle of attack and angle of bank), the entry path inclination and the flight time being free. Two transfer maneuvers are considered: (DA) direct ascent to LEO; (IA) indirect ascent to LEO via PEO.

While the motion of the AFE spacecraft in a 3D-space is described by a system of six ODEs, substantial simplifications are possible if one exploits the smallness of three key quantities: the change of orbital inclination; the bank angle; and the Earth's angular velocity. Indeed, the complete system can be decoupled into two subsystems, one describing the longitudinal motion and one describing the lateral motion.

The angle of attack history, the entry path inclination, and the flight time are determined via the longitudinal motion subsystem; in this subsystem, the total characteristic velocity is minimized subject to the specified LEO requirement. The angle of bank history is determined via the lateral motion subsystem; in this subsystem, the difference between the instantaneous bank angle and a constant bank angle is minimized in the least square sense subject to the specified orbital inclination requirement.

From the extensive numerical computations, the following conclusions were obtained:

(i) The optimal trajectories are one-subarc trajectories, with constant angle of attack and constant angle of bank. Specifically, α = 17.0 deg and μ = 5.14 deg.

(ii) Throughout the atmospheric pass, the (α,μ)-pair yields a negative vertical component of the lift, which offsets the centrifugal force effects due to the curvature of the Earth, so as to ensure exit conditions compatible with the specified LEO.

(iii) Throughout the atmospheric pass, the (α,μ)-pair yields a horizontal component of the lift which nearly offsets the effects due to the Earth's rotation. In this way, the instantaneous orbital plane is almost identical with the initial orbital plane, meaning that the wedge angle is nearly zero. This means that, for efficient flight, the motion of the AFE spacecraft is nearly planar in an inertial space; in other words, one must avoid energy dissipation associated with the lateral motion.

(iv) In an inertial reference frame, the entry path inclination is $\tilde{\gamma}_0$ = -4.13 deg, thus yielding trajectories about 0.36 deg flatter than both the nominal trajectory of Ref. 8 and the optimal trajectories of Ref. 14. In turn, this results in higher minimum altitude, lower peak dynamic pressure, and lower peak heating rate.

References

1. WALBERG, G. D., A Survey of Aeroassisted Orbital Transfer, Journal of Spacecraft and Rockets, Vol. 22, No. 1, pp. 3-18, 1985.

2. MEASE, K. D., and VINH, N. X., Minimum-Fuel Aeroassisted Coplanar Orbit Transfer Using Lift Modulation, Journal of Guidance, Control, and Dynamics, Vol. 8, No. 1, pp. 134-141, 1985.

3. MIELE, A., and VENKATARAMAN, P., Optimal Trajectories for Aeroassisted Orbital Transfer, Acta Astronautica, Vol. 11, Nos. 7-8, pp. 423-433, 1984.

4. MIELE, A., and BASAPUR, V. K., Approximate Solutions to Minimax Optimal Control Problems for Aeroassisted Orbital Transfer, Acta Astronautica, Vol. 12, No. 10, pp. 809-818, 1985.

5. MIELE, A., BASAPUR, V. K., and MEASE, K. D., Nearly-Grazing Optimal Trajectories for Aeroassisted Orbital Transfer, Journal of the Astronautical Sciences, Vol. 34, No. 1, pp. 3-18, 1986.

6. MIELE, A., BASAPUR, V. K., and LEE, W. Y., Optimal Trajectories for Aeroassisted, Coplanar Orbital Transfer, Journal of Optimization Theory and Applications, Vol. 52, No. 1, pp. 1-24, 1987.

7. MIELE, A., WANG, T., and DEATON, A. W., Properties of the Optimal Trajectories for Coplanar, Aeroassisted Orbital Transfer, Rice University, Aero-Astronautics Report No. 249, 1990.

8. ANONYMOUS, N. N., Aeroassisted Flight Experiment: Preliminary Design Document, NASA Marshall Space Flight Center, 1986.

9. GAMBLE, J. D., CERIMELE, C. J., MOORE, T. E., and HIGGINS, J., Atmospheric Guidance Concepts for an Aeroassist Flight Experiment, Journal of the Astronautical Sciences, Vol. 36, Nos. 1-2, pp. 45-71, 1988.

10. MIELE, A., ZHAO, Z. G., and LEE, W. Y., Optimal Trajectories for the Aeroassisted Flight Experiment, Part 1, Equations of Motion in an Earth-Fixed System, Rice University, Aero-Astronautics Report No. 238, 1989.

11. MIELE, A., ZHAO, Z. G., and LEE, W. Y., Optimal Trajectories for the Aeroassisted Flight Experiment, Part 2, Equations of Motion in an Inertial System, Rice University, Aero-Astronautics Report No. 239, 1989.

12. MIELE, A., WANG, T., LEE, W. Y., and ZHAO, Z. G., Optimal Trajectories for the Aeroassisted Flight Experiment, Part 3, Formulation, Results, and Analysis, Rice University, Aero-Astronautics Report No. 242, 1989.

13. MIELE, A., WANG, T., LEE, W. Y., WANG, H., and WU, G. D., Optimal Trajectories for the Aeroassisted Flight Experiment, Part 4, Data, Tables, and Graphs, Rice University, Aero-Astronautics Report No. 243, 1989.

14. MIELE, A., WANG, T., LEE, W. Y., and ZHAO, Z. G., Optimal Trajectories for the Aeroassisted Flight Experiment, Paper No. IAF-89-361, 40th Congress of the International Aeronautical Federation, Malaga, Spain, 1989.

15. NOAA, NASA, and USAF, US Standard Atmosphere, 1976, US Government Printing Office, Washington, DC, 1976.

16. MIELE, A., WANG, T., and BASAPUR, V. K., Primal and Dual Formulations of Sequential Gradient-Restoration Algorithms for Trajectory Optimization Problems, Acta Astronautica, Vol. 13, No. 8, pp. 491-505, 1986.

17. MIELE, A., and WANG, T., Primal-Dual Properties of Sequential Gradient-Restoration Algorithms for Optimal Control Problems, Part 1, Basic Problem, Integral Methods in Science and Engineering, Edited by F. R. Payne et al, Hemisphere Publishing Corporation, Washington, DC, pp. 577-607, 1986.

18. MIELE, A., and WANG, T., Primal-Dual Properties of Sequential Gradient-Restoration Algorithms for Optimal Control Problems, Part 2, General Problem, Journal of Mathematical Analysis and Applications, Vol. 119, Nos. 1-2, pp. 21-54, 1986.

19. MIELE, A., and IYER, R. R., General Technique for Solving Nonlinear, Two-Point Boundary-Value Problems via the Method of Particular Solutions, Journal of Optimization Theory and Applications, Vol. 5, No. 5, pp. 382-399, 1970.

20. MIELE, A., and IYER, R. R., Modified Quasilinearization Method for Solving Nonlinear, Two-Point Boundary-Value Problems, Journal of Mathematical Analysis and Applications, Vol. 36, No. 3, pp. 674-692, 1971.

21. MIELE, A., NAQVI, S., LEVY, A. V., and IYER, R. R., Numerical Solution of Nonlinear Equations and Nonlinear, Two-Point Boundary-Value Problems, Advances in Control Systems, Edited by C. T. Leondes, Academic Press, New York, New York, Vol. 8, pp. 189-215, 1971.

List of Tables

Table 1. AFE spacecraft, aerodynamic data.

α(deg)	C_L	C_D	C_L/C_D	C_M
7	-0.2088	1.5078	-0.1385	0.0295
9	-0.2473	1.4826	-0.1668	0.0232
11	-0.2842	1.4555	-0.1953	0.0171
13	-0.3187	1.4258	-0.2235	0.0113
15	-0.3512	1.3915	-0.2524	0.0054
17	-0.3807	1.3549	-0.2810	-0.0004
19	-0.4065	1.3132	-0.3095	-0.0064
21	-0.4283	1.2688	-0.3376	-0.0123
23	-0.4458	1.2187	-0.3658	-0.0181
25	-0.4595	1.1683	-0.3933	-0.0235
27	-0.4707	1.1182	-0.4210	-0.0287

Table 2. Effect of the control bounds, main properties.

Quantity	DAOT Case (i)	DAOT Case (ii)	DAOT Case (iii)	Units
N_s	0	0	0	-
τ	1045	845	689	sec
α	27.0	17.0	10.0	deg
C_L	-0.47	-0.38	-0.27	-
μ	3.45	5.14	8.18	deg
min(h)	78.6	78.1	77.3	km
max(DP)	991	1040	1160	N/m^2
max(HR)	134	135	141	W/cm^2
$\tilde{\gamma}_0$	-4.08	-4.13	-4.20	deg
$\max\lvert\Delta\tilde{i}\rvert$	0.01	0.01	0.01	deg
$\max\lvert\Delta\tilde{\Omega}\rvert$	0.01	0.01	0.01	deg
$\max(\tilde{\eta})$	0.01	0.01	0.01	deg
$\Delta\tilde{V}_{00}$	1.490	1.490	1.490	km/sec
$\Delta\tilde{V}_{11}$	0.070	0.072	0.075	km/sec
$\Delta\tilde{V}$	1.560	1.562	1.565	km/sec

Table 3. Comparison of AFE trajectories, main properties.

Quantity	DAOT Case (ii)	IAOT Case (ii)	IART	Units
N_s	0	0	4	-
τ	845	821	486	sec
α	17.0	17.0	17.0	deg
C_L	-0.38	-0.38	-0.38	-
μ	5.14	5.14	(*)	deg
min(h)	78.1	78.1	74.8	km
max (DP)	1040	1039	1578	N/m^2
max(HR)	135	135	156	W/cm^2
$\tilde{\gamma}_0$	-4.13	-4.13	-4.49	deg
$\max\lvert\Delta\tilde{i}\rvert$	0.01	0.01	1.08	deg
$\max\lvert\Delta\tilde{\Omega}\rvert$	0.01	0.01	0.31	deg
$\max(\tilde{\eta})$	0.01	0.01	1.08	deg
$\Delta\tilde{V}_{00}$	1.490	1.490	1.491	km/sec
$\Delta\tilde{V}_{22}$	0.000	0.072	0.088	km/sec
$\Delta\tilde{V}_{11}$	0.072	0.010	0.010	km/sec
$\Delta\tilde{V}$	1.562	1.572	1.589	km/sec

(*) Values of μ_1, μ_2, μ_3, μ_4, μ_5 are given by Eqs. (39).

Table 4. Comparison of AFE trajectories, entry conditions.

Quantity	DAOT Case(ii)	IAOT Case (ii)	IART	Units
θ_0	-134.52	-134.52	-134.52	deg
$\tilde{\theta}_0$	-134.52	-134.52	-134.52	deg
ϕ_0	-4.49	-4.49	-4.49	deg
h_0	122	122	122	km
r_0	6500	6500	6500	km
V_0	9.906	9.906	9.895	km/sec
$\tilde{V}_0$	10.308	10.308	10.308	km/sec
γ_0	-4.296	-4.296	-4.675	deg
$\tilde{\gamma}_0$	-4.128	-4.128	-4.487	deg
χ_0	-29.42	-29.42	-29.42	deg
$\tilde{\chi}_0$	-28.13	-28.13	-28.13	deg
i_0	29.73	29.73	29.73	deg
$\tilde{i}_0$	28.45	28.45	28.45	deg
Ω_0	-126.62	-126.62	-126.62	deg
$\tilde{\Omega}_0$	-126.19	-126.19	-126.19	deg
η_0	0.00	0.00	0.00	deg
$\tilde{\eta}_0$	0.00	0.00	0.00	deg

Table 5. Comparison of AFE trajectories, exit conditions.

Quantity	DAOT Case (ii)	IAOT Case (ii)	IART	Units
θ_1	-78.90	-80.50	-103.31	deg
$\tilde{\theta}_1$	-75.37	-77.07	-101.28	deg
ϕ_1	22.79	22.28	12.84	deg
h_1	122	122	122	km
r_1	6500	6500	6500	km
V_1	7.481	7.491	7.462	km/sec
$\tilde{V}_1$	7.882	7.892	7.876	km/sec
γ_1	0.803	0.860	1.358	deg
$\tilde{\gamma}_1$	0.762	0.816	1.287	deg
χ_1	-18.52	-19.21	-27.15	deg
$\tilde{\chi}_1$	-17.52	-18.17	-25.61	deg
i_1	29.05	29.10	29.82	deg
$\tilde{i}_1$	28.46	28.46	28.46	deg
Ω_1	-128.04	-127.92	-126.74	deg
$\tilde{\Omega}_1$	-126.20	-126.20	-126.16	deg
η_1	0.97	0.90	0.11	deg
$\tilde{\eta}_1$	0.00	0.00	0.02	deg

List of Figures

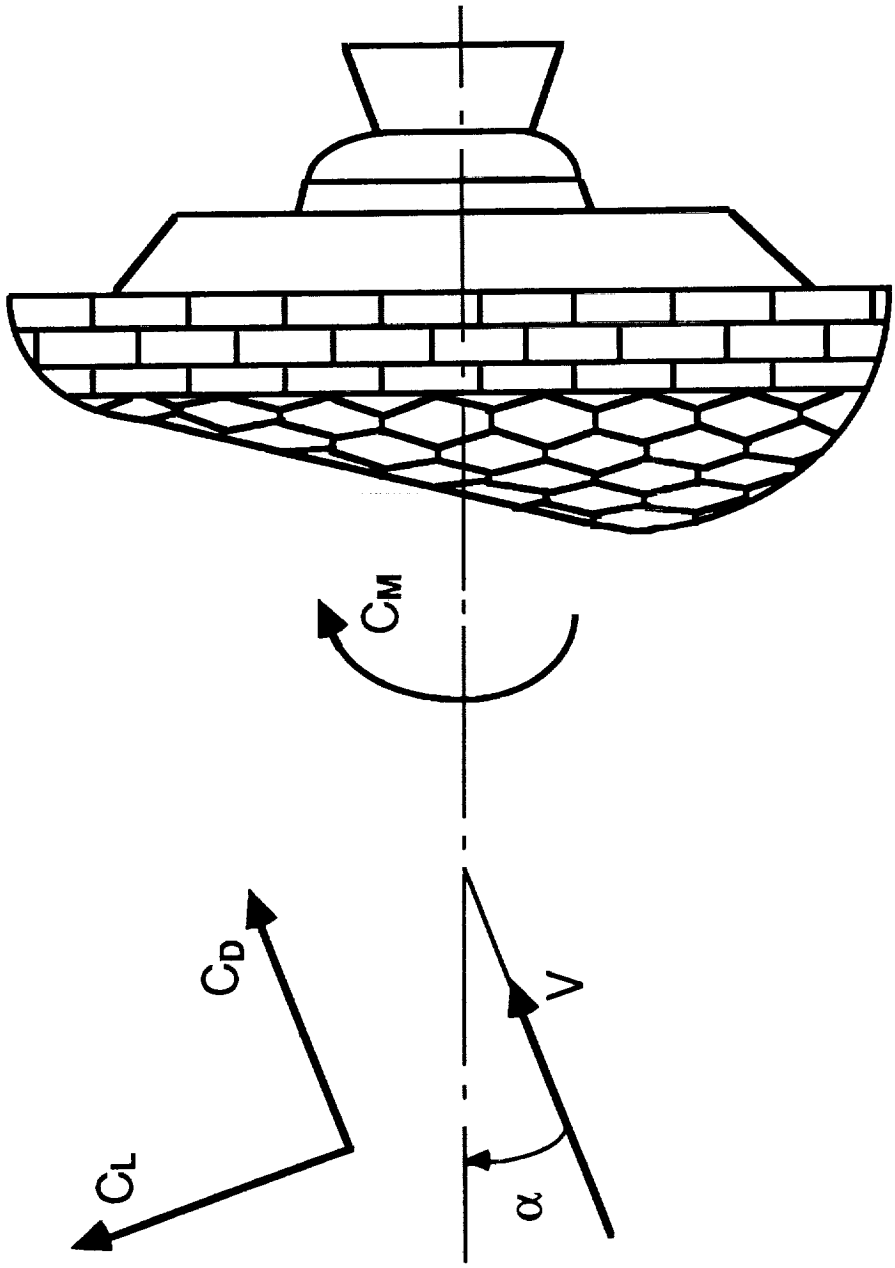

FIG. 1. AFE RAKED-CONE CONFIGURATION.

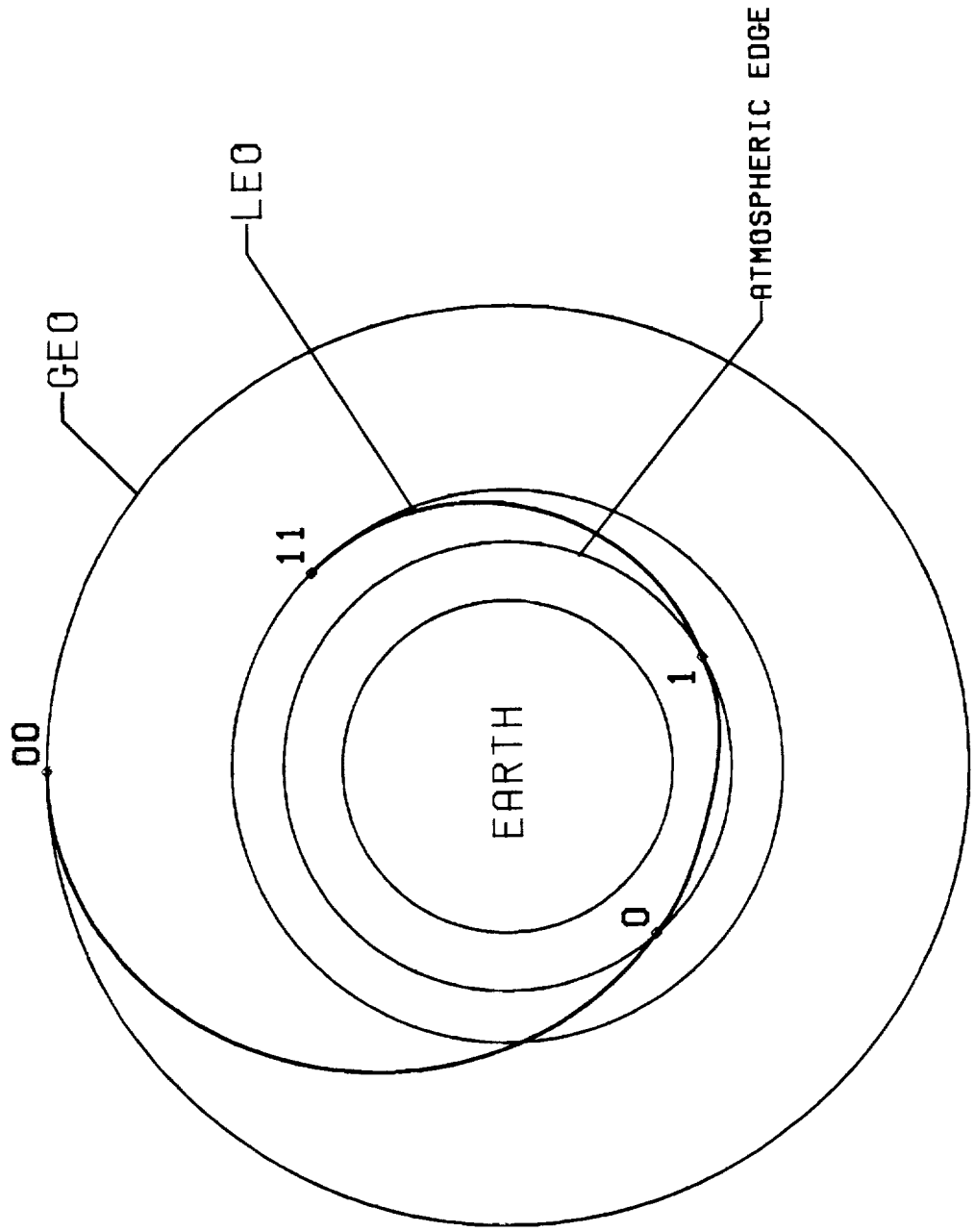

FIG. 2A. COPLANAR, AEROASSISTED ORBITAL TRANSFER: DIRECT ASCENT.

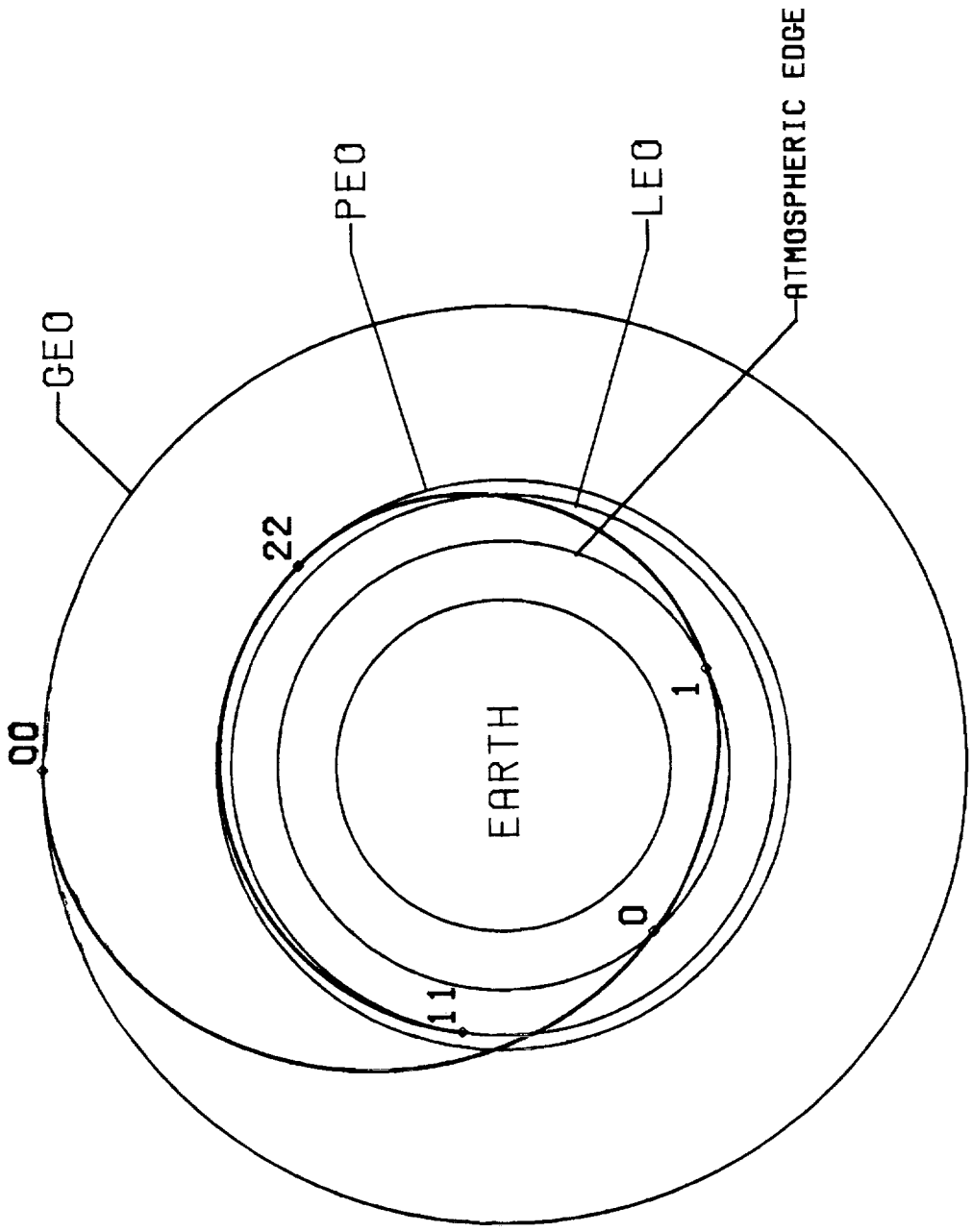

FIG. 2B. COPLANAR, AEROASSISTED ORBITAL TRANSFER: INDIRECT ASCENT.

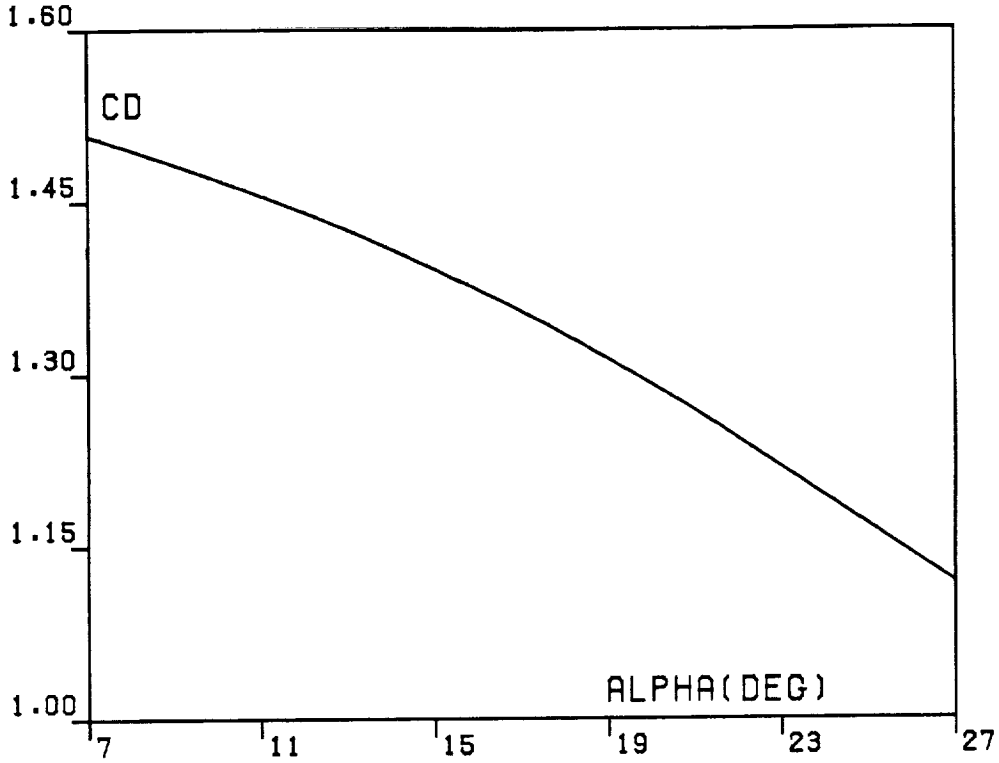

FIG. 3A. DRAG COEFFICIENT.

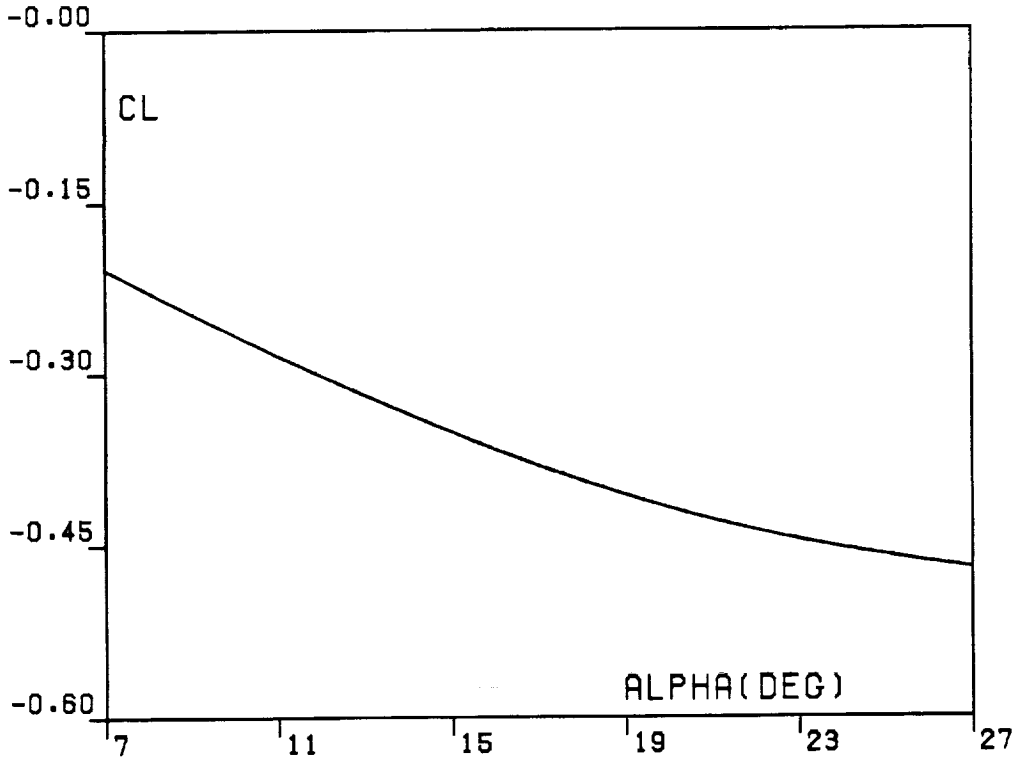

FIG. 3B. LIFT COEFFICIENT.

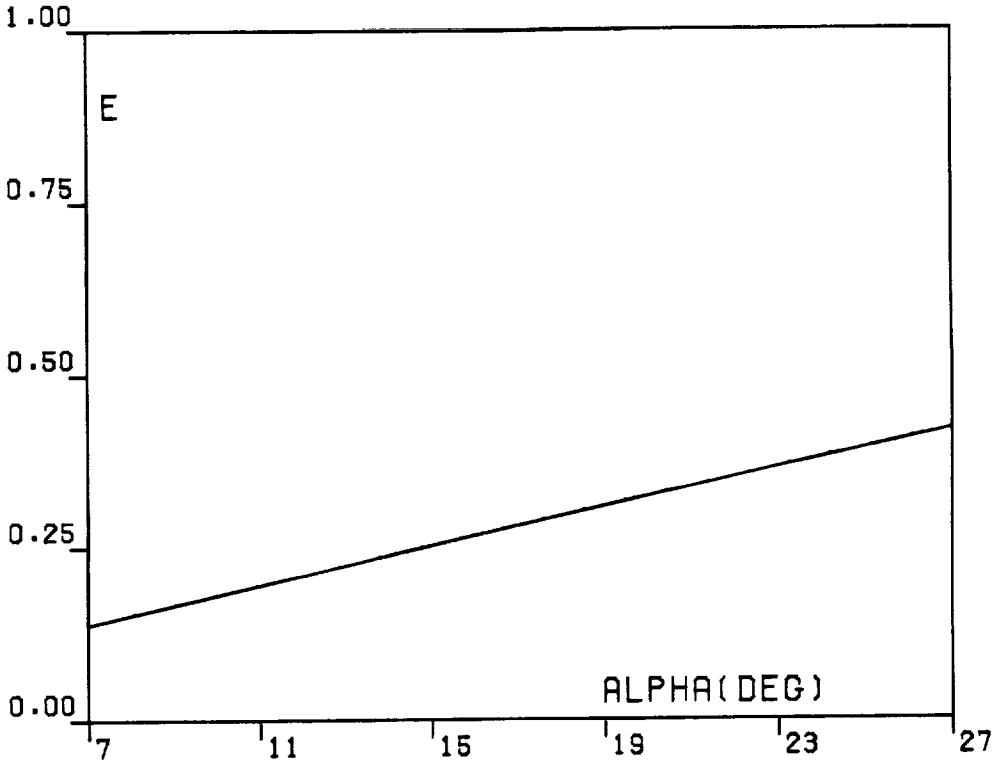

FIG. 3C. LIFT-TO-DRAG RATIO MODULUS.

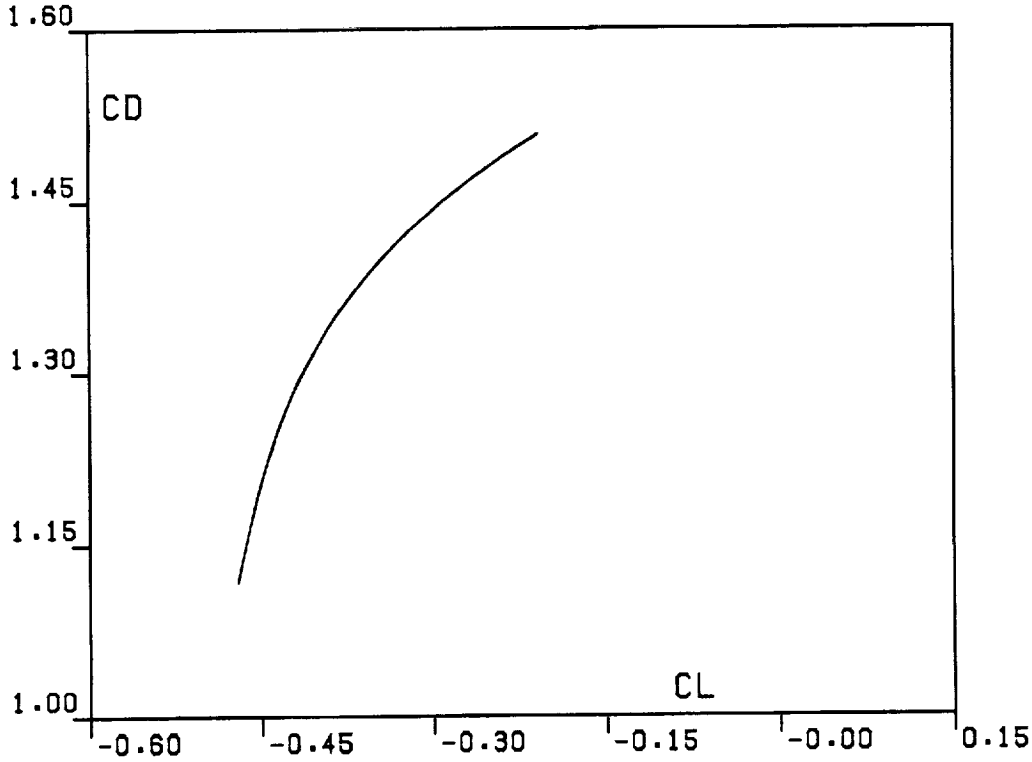

FIG. 3D. DRAG POLAR.

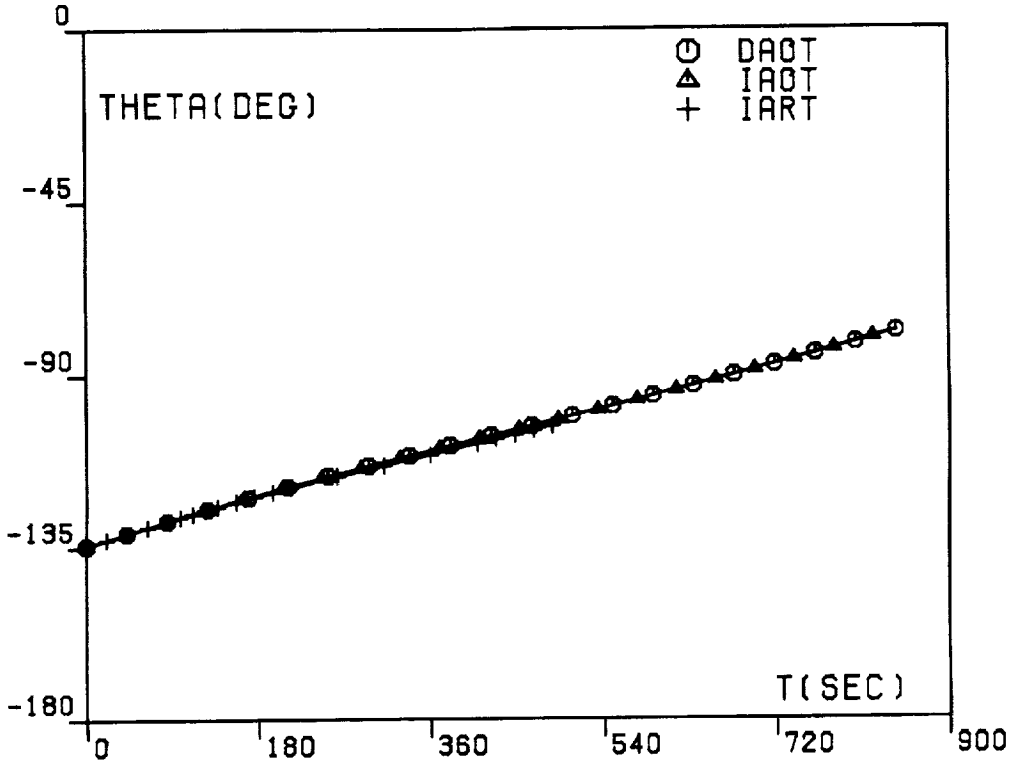

FIG. 4A. AFE TRAJECTORIES, RELATIVE LONGITUDE.

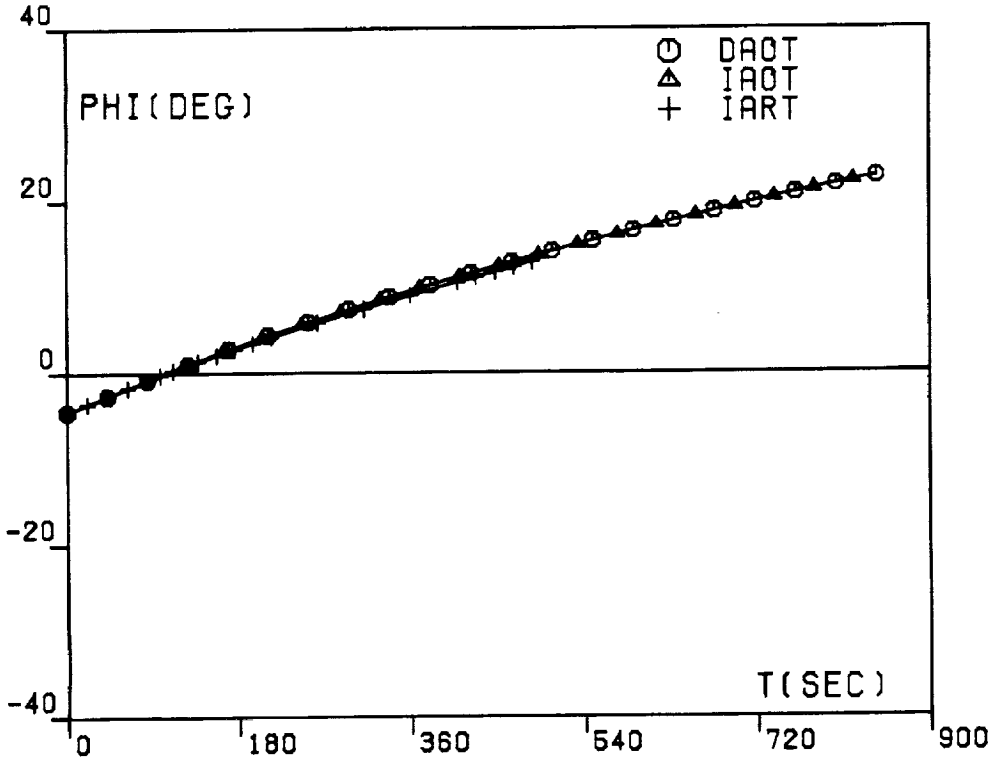

FIG. 4B. AFE TRAJECTORIES, LATITUDE.

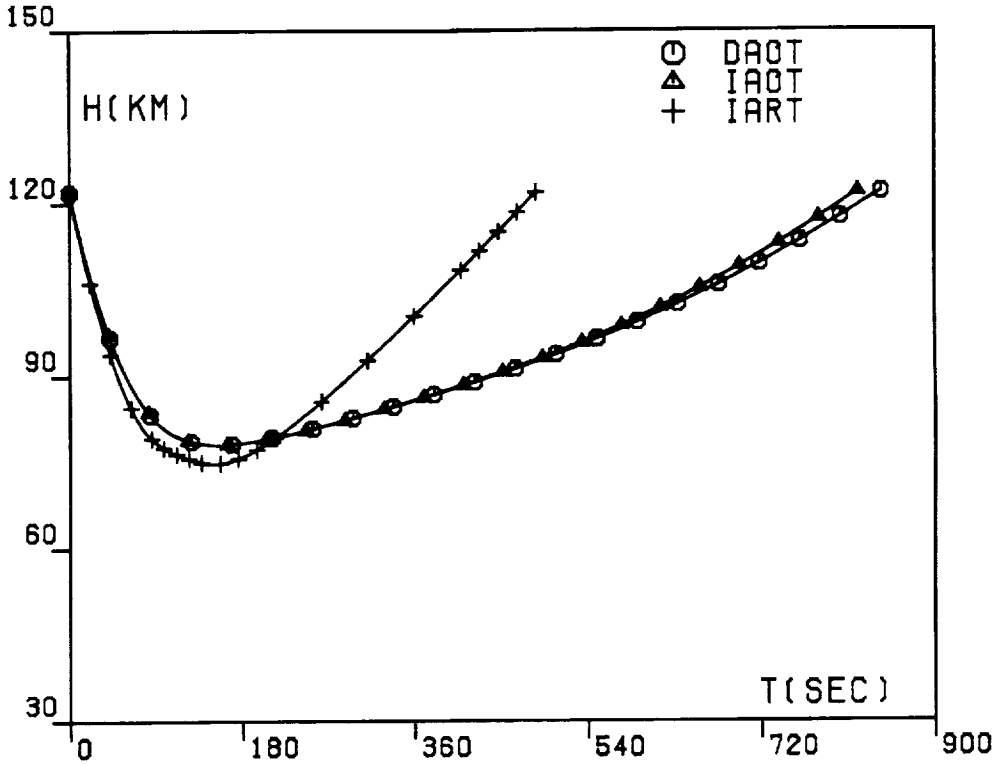

FIG. 4C. AFE TRAJECTORIES. ALTITUDE.

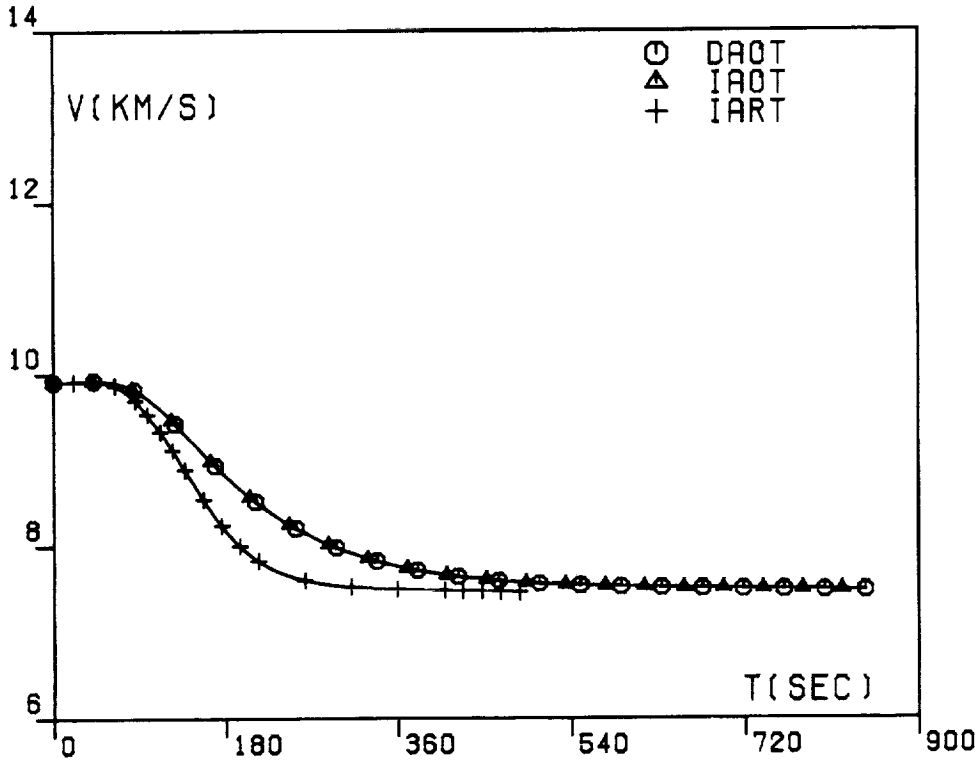

FIG. 4D. AFE TRAJECTORIES. RELATIVE VELOCITY.

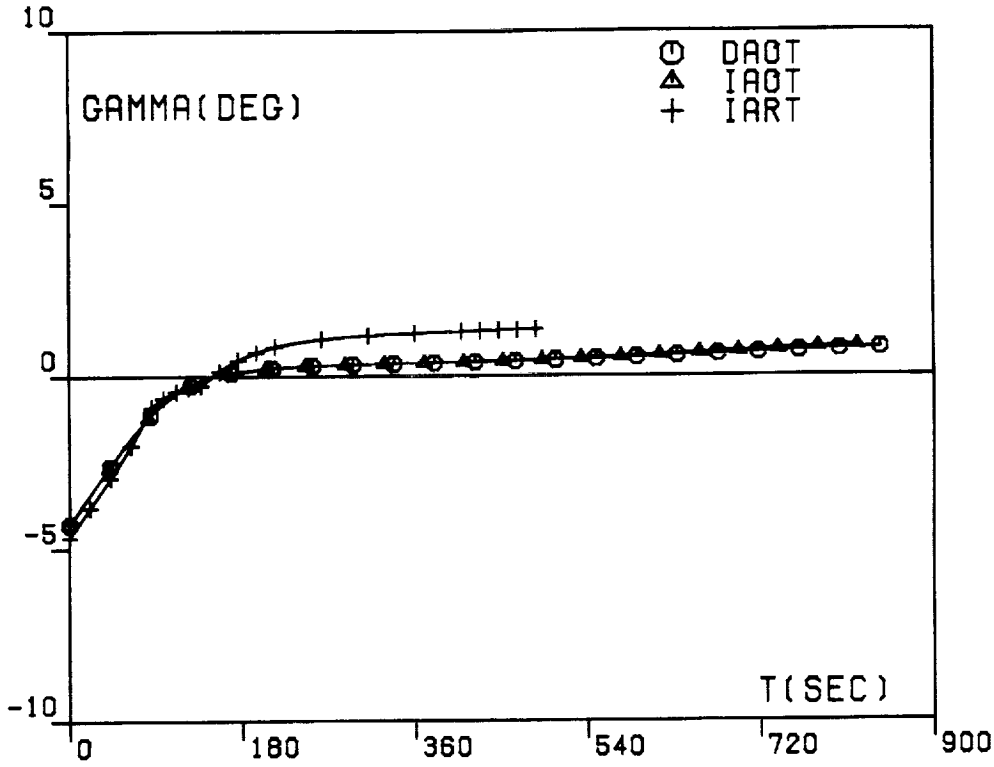

FIG. 4E. AFE TRAJECTORIES,
RELATIVE PATH INCLINATION.

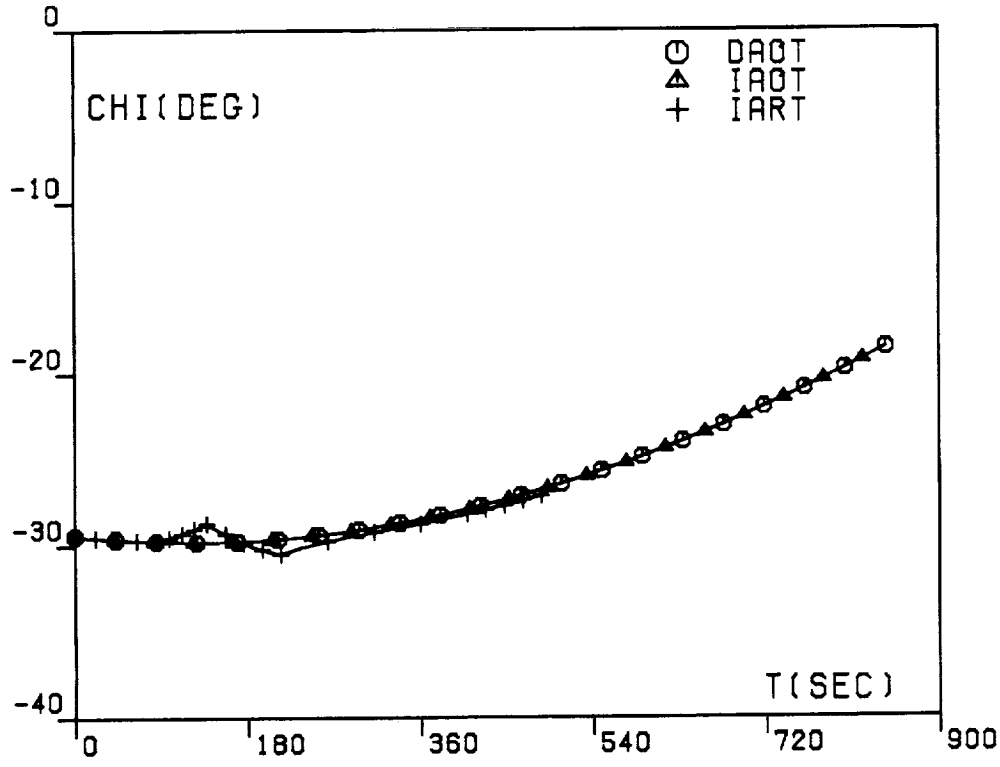

FIG. 4F. AFE TRAJECTORIES,
RELATIVE HEADING ANGLE.

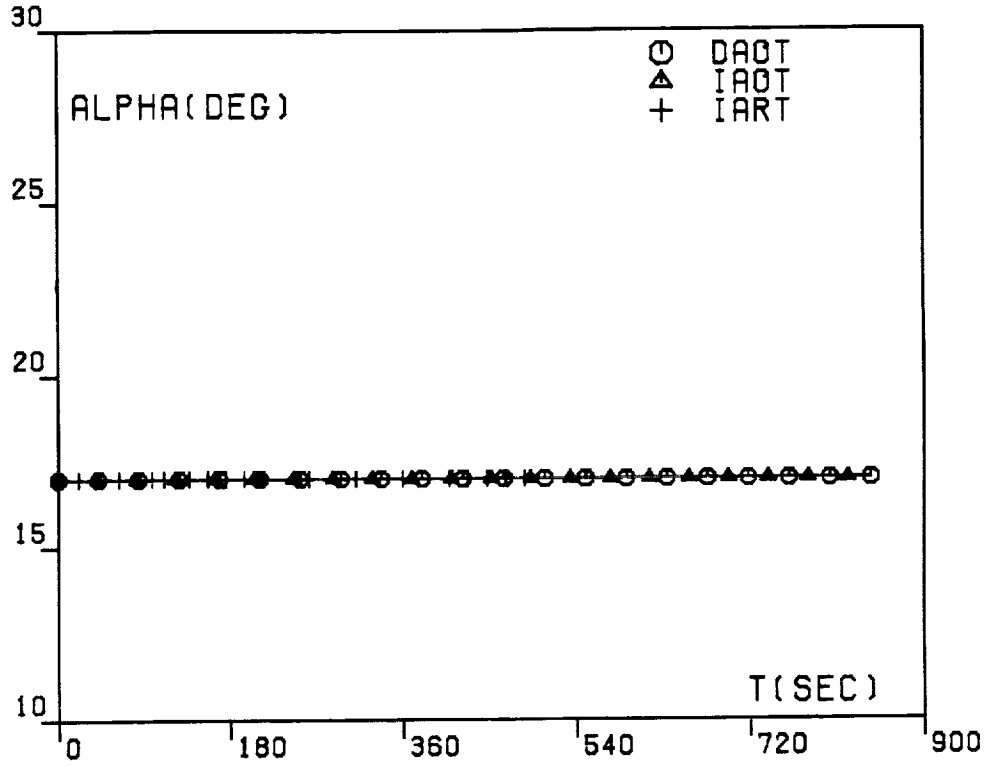

FIG. 4G. AFE TRAJECTORIES.
ANGLE OF ATTACK.

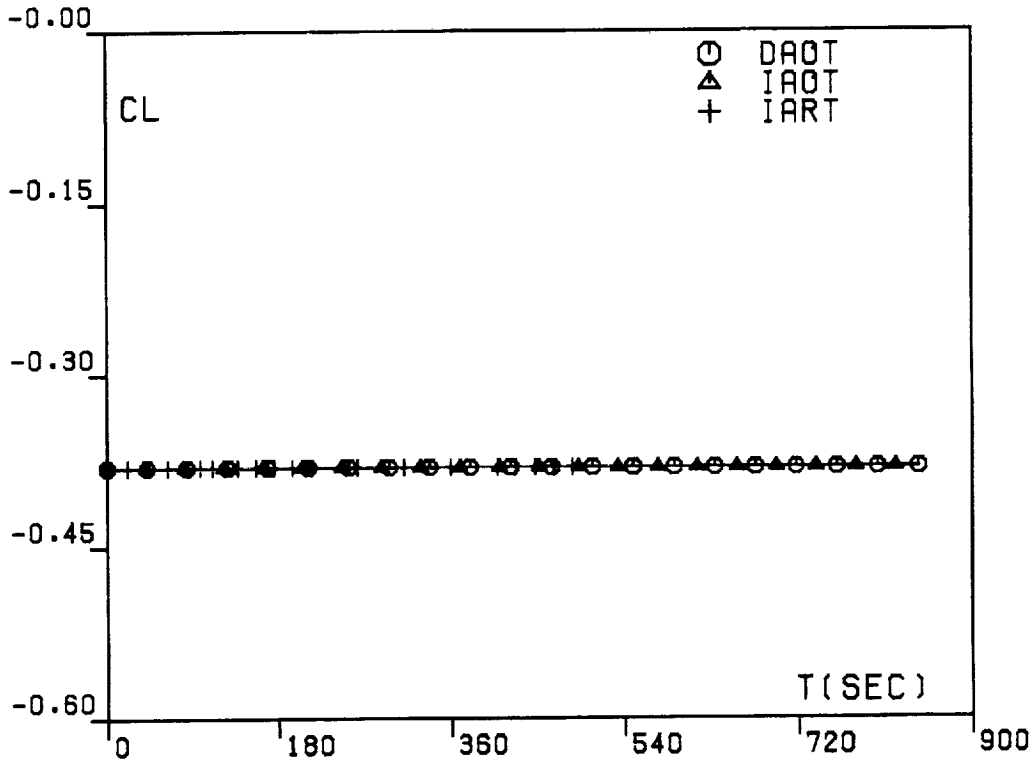

FIG. 4H. AFE TRAJECTORIES.
LIFT COEFFICIENT.

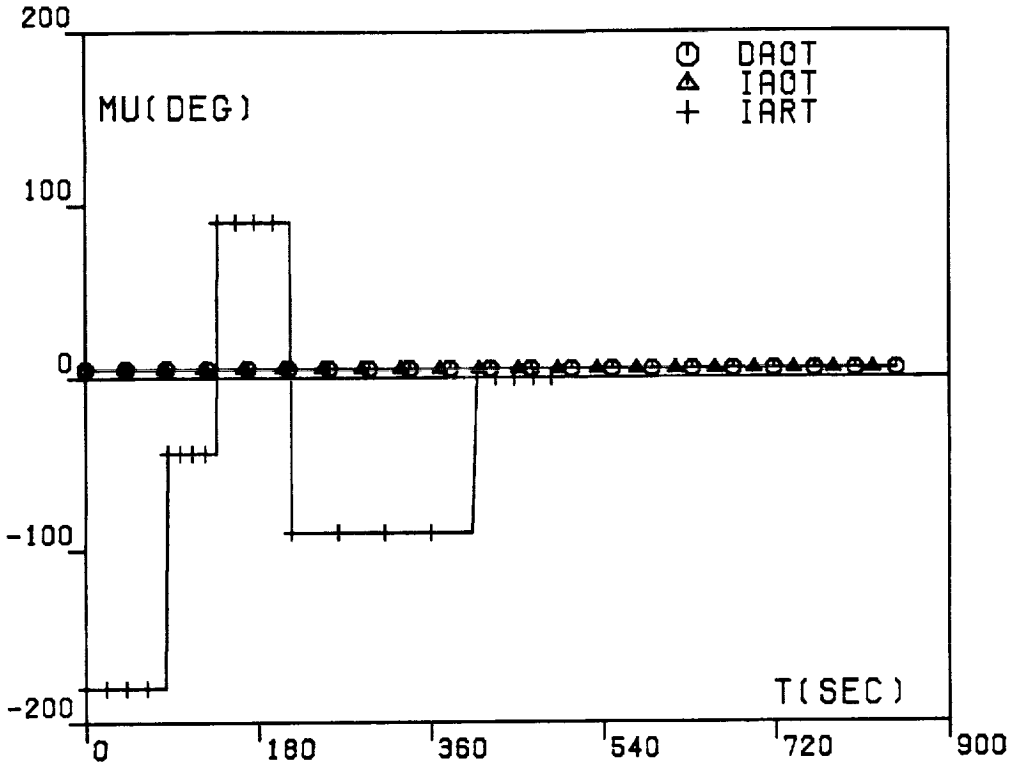

FIG. 4I. AFE TRAJECTORIES, BANK ANGLE.

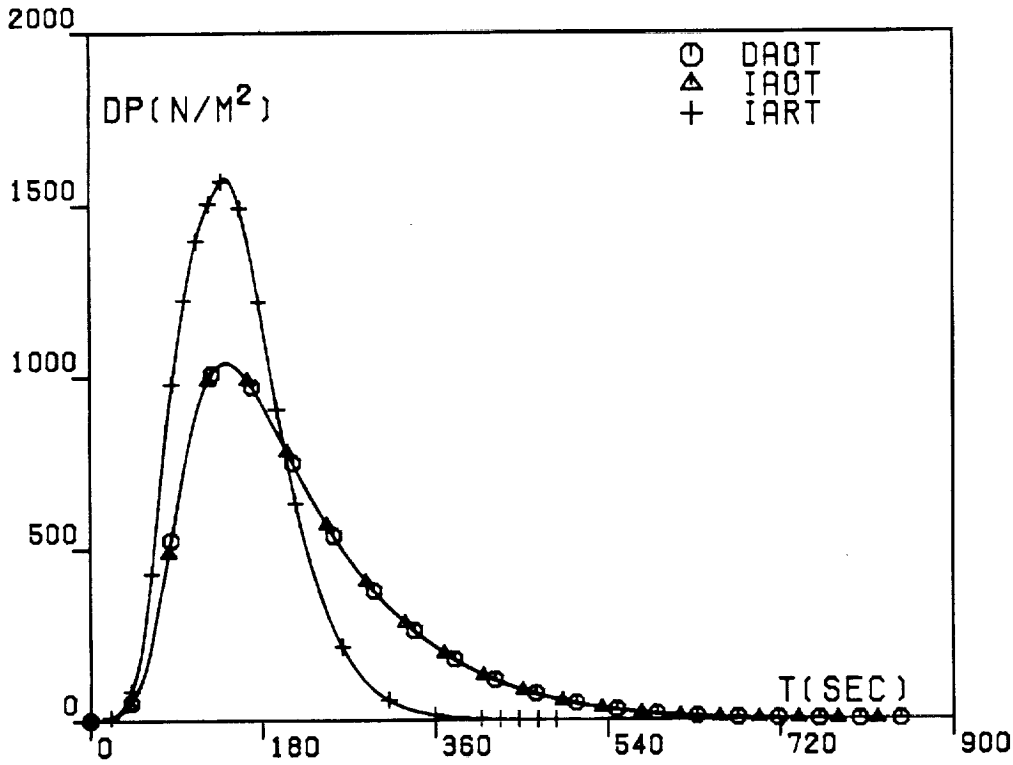

FIG. 4J. AFE TRAJECTORIES, DYNAMIC PRESSURE.

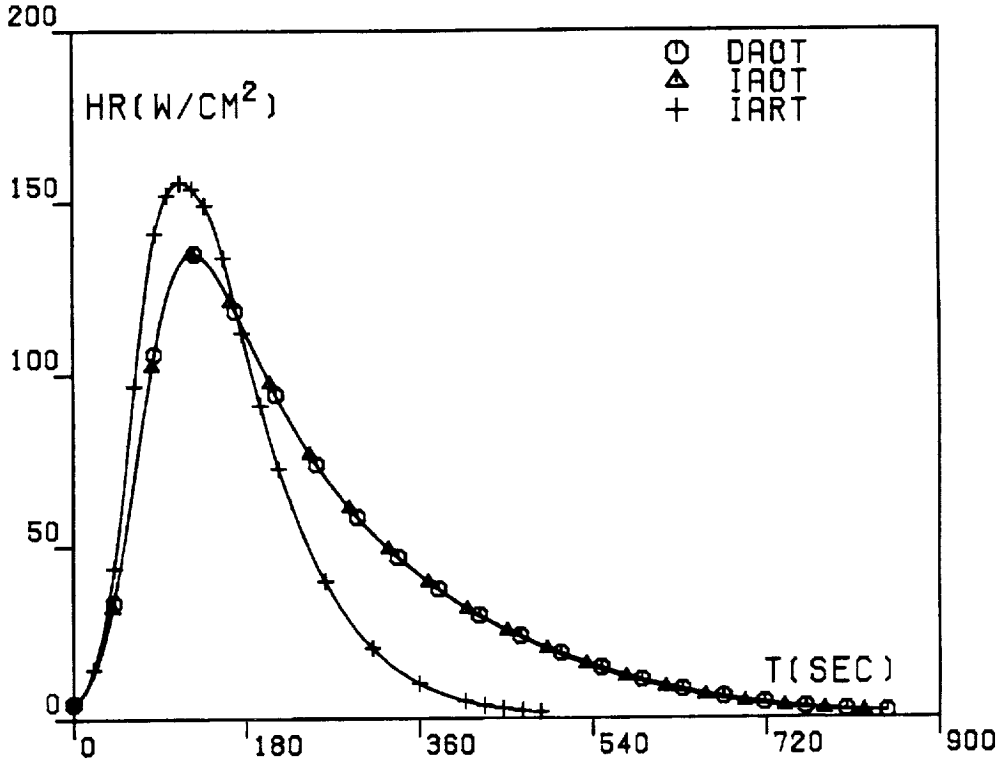

FIG. 4K. AFE TRAJECTORIES.
HEATING RATE.

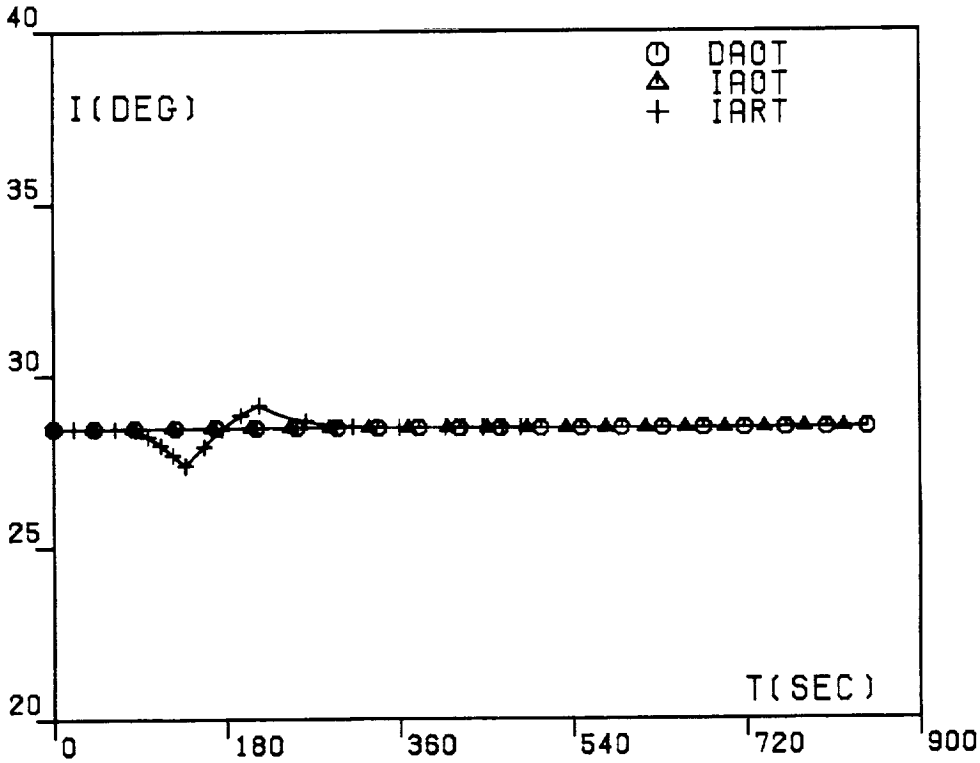

FIG. 4L. AFE TRAJECTORIES.
INERTIAL ORBITAL INCLINATION.

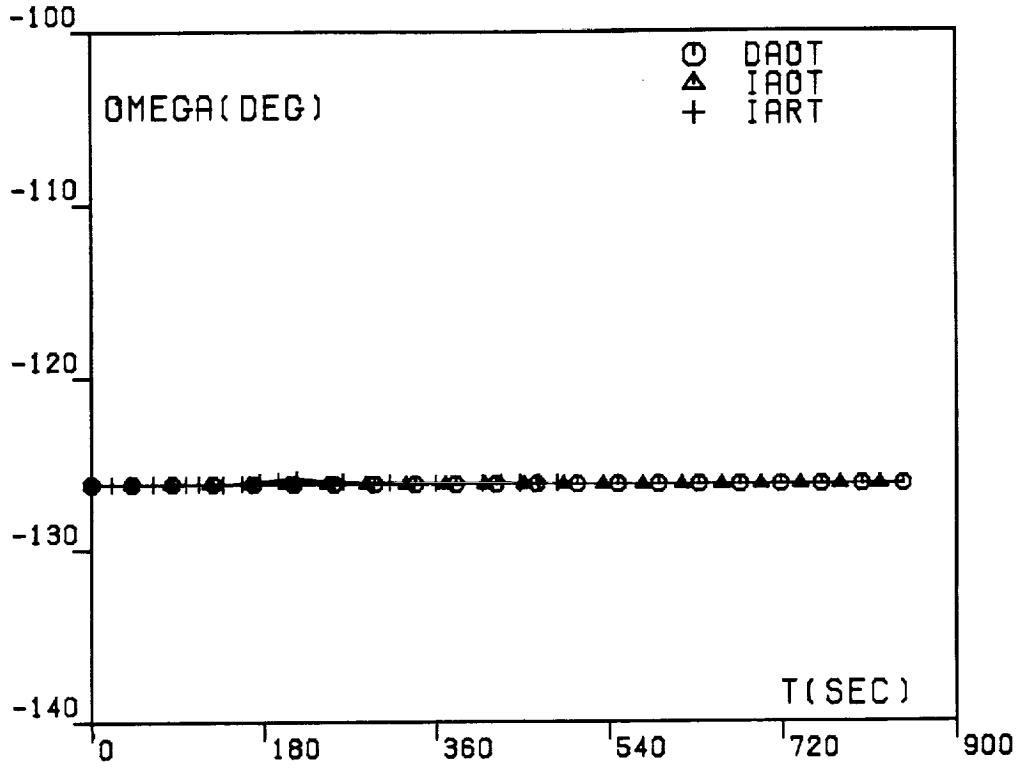

FIG. 4M. AFE TRAJECTORIES. INERTIAL LONGITUDE OF ASCENDING NODE.

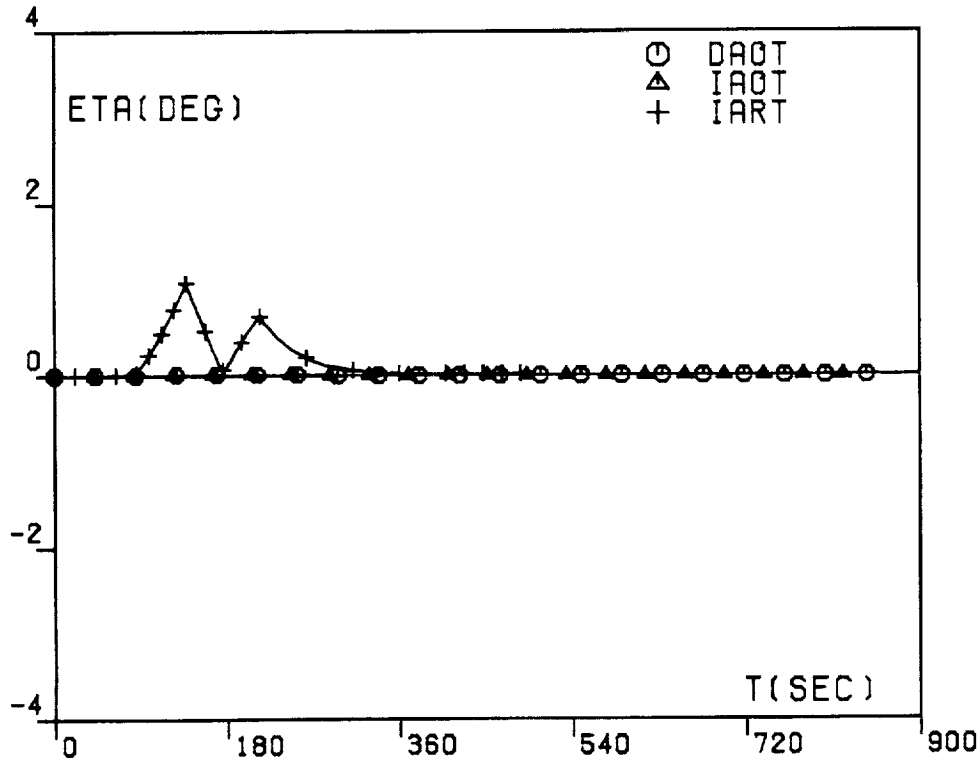

FIG. 4N. AFE TRAJECTORIES. INERTIAL WEDGE ANGLE.